Analysis of the photocurrent action spectra of MEH-PPV polymer photodiodes

M. G. Harrison and J. Grüner
Cavendish Laboratory, Madingley Road, Cambridge CB3 0HE, United Kingdom

G. C. W. Spencer
University Chemical Laboratory, Lensfield Road, Cambridge CB2 1EW, United Kingdom

(Received 17 October 1996; revised manuscript received 7 November 1996)

We have measured the photocurrent action spectra of the conjugated polymers poly[2-methoxy, 5 ethyl (2′ hexyloxy) paraphenylenevinylene] (MEH-PPV) and poly(phenylenevinylene) (PPV) in sandwich cells between indium tin oxide (ITO) and aluminum electrodes. Under forward bias and illumination through ITO, the photocurrent spectrum is broad and has a maximum at high energy, where the absorption coefficient is greatest (the *symbatic* response). Under reverse bias and illumination through ITO, the photocurrent spectrum consists of a very narrow peak (the full width at half maximum is 0.1 eV), located in the low-energy tail of the absorption profile (the *antibatic* response). Several established models attempt to explain this behavior and to relate the photocurrent action spectrum to the absorption coefficient, considering penetration depth of the light and diffusion of excitons or directly photogenerated charges. At a qualitative level many of these seem to provide an adequate description. In this paper, we undertake a quantitative examination of these models and we find that none of them can reproduce the very narrow antibatic response that we observe in both MEH-PPV and PPV. Upon exposure to air, we observe an enhancement of the photocurrent by a much greater factor than the dark current, from which we conclude that charge generation is mediated by exciton dissociation. As the temperature decreases we observe a progressive redshift of the absorption edge, although the photocurrent onset undergoes a much smaller redshift. We therefore conclude that the narrow antibatic peak is due to a specific enhancement of dissociation upon excitation at low energy. We propose that the particularly sharp onset of photocurrent at low energy may be due to enhanced intermolecular charge separation within crystallite grains between those neighboring conjugated segments that are more extended and more planar. [S0163-1829(97)07811-9]

I. INTRODUCTION

Since the discovery of electroluminescence in conjugated polymers,[1] increasing research activity has been directed toward investigating the semiconductor physics of these materials and their potential applications in optoelectronic devices, including field-effect transistors,[2] optical modulators,[3,4] and solar cells,[5–7] largely motivated by the ease of preparing thin semiconductor films by solution processing and the ability to tune the semiconductor energy gap by grafting chemical substituents to the polymer backbone.

Theoretical models which successfully describe the physics of inorganic semiconductors have been applied to conjugated polymers with some success. However, it is always important to remember that there are large differences between the three-dimensional crystal lattice of most inorganic semiconductors and the crystalline-amorphous structure of conjugated polymers, in which polymer chains are weakly bound together by van der Waals forces. Although electric charge is delocalized along π-conjugated segments of the polymer backbone, the length of such perfectly conjugated segments is typically limited to length scales of around 5 nm, and hence charges also need to move between chains in order to percolate through a thin-film device, which is typically a few hundred nm thick. Hence the charge-transport and semiconducting properties of these materials are sensitive to the morphology of the polymer chains and the local structural order within the film. This is a key idea in this work, and we discuss it in more detail below.

Furthermore, electronic charge is not present as free electrons or holes, but as polaronic species; the geometry of chemical bonds is distorted in the vicinity of an electric charge (lattice relaxation). For conjugated oligomers, at least three species of charged excitation have been identified, namely, monovalent polarons (or radical cations) and divalent charge carriers, such as bipolarons (intramolecular dications) and also π stacks or π dimers (intermolecular dications).[8,9] These species can have vastly different mobilities, and the equilibrium between them is sensitive to temperature,[10,11] structural order (also temperature-dependent),[8,9,12] and the presence of impurities.[13,14] Hence, also for these reasons, there is a need for some caution when transposing the theory of inorganic semiconductor physics to conjugated polymers.

It remains a controversial issue whether it is appropriate to describe conjugated polymers by a traditional semiconductor band model, or whether it is necessary to remember the molecular nature of the material and consider the role of the Coulomb attraction between positive and negative charges in bound electron-hole pairs, or excitons. The spectral response of the photocurrent has often been used to argue in favor of one model or the other. In highly crystalline polydiacetylenes, there is a large energy difference of at least 0.5 eV between the onset of absorption and the onset of photoconductivity,[15] and this is widely accepted as evidence of the importance of electron-electron interactions in this

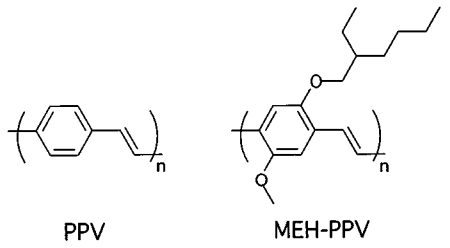

FIG. 1. Structural formulas for unsubstituted poly(*para*-phenylenevinylene) (PPV) and its soluble derivative, poly[2-methoxy, 5 ethyl (2′hexyloxy) *para*-phenylenevinylene] (MEH-PPV).

material.[16] For poly(phenylenevinylene)'s (PPV's) the onsets of photoconductivity and absorption usually occur at similar energy.[17–23] This has been cited as evidence of a semiconducting band model,[21,24] with direct photogeneration of free positive and negative carriers, although this interpretation is in conflict with photoconduction in many organic semiconductors,[25,26] in which charge generation is a secondary process, resulting from dissociation of the exciton by interaction with interfaces and electrodes, defects, impurities, and oxygen. We have briefly reported some of our key results elsewhere.[27] In this paper, we make a critical assessment of the existing models for the photocurrent action spectra, and note a number of additional factors which should be considered in the development of a model which could provide a more quantitative description for conjugated polymers. In particular, we focus on the sharp rise of the photocurrent which is usually observed at the low energy tail of absorption. We also discuss the implications of our results in terms of the debate between excitons and the semiconductor band model.

II. EXPERIMENTAL DETAILS

A. Device fabrication

The diodes were fabricated in the usual single-layer sandwich structure. We used glass substrates, coated with transparent, conducting indium tin oxide (ITO) to serve as the anode. The ITO-coated glass was etched to define a hole-injecting electrode, approximately 8 mm wide. Thin films of poly(2-methoxy, 5 ethyl (2′hexyloxy) paraphenylenevinylene) (MEH-PPV) were deposited by spin coating, to give film thicknesses in the range 100–800 nm, as measured by a Dektak II surface profilometer. For diodes made with PPV, films were deposited by spin coating from the soluble tetrahydrothiophenium precursor solution, followed by thermal conversion at 220 °C, for 12 h under vacuum. The structural formulas of unsubstituted PPV, and its soluble derivative MEH-PPV, are shown in Fig. 1. Finally, the metal cathodes were deposited by evaporation. As cathode materials, we used calcium, magnesium, aluminum, semitransparent aluminum, and semitransparent gold. We fabricated eight pixels per substrate, each of area approximately 6 mm^2. We used relatively thin polymer films because we previously observed spurious spectral features when using very thick films, which we attributed to optical interference effects; these could be suppressed by tilting the device, so that the irradiation was at glancing incidence to the substrate, thus reducing the density of multiple reflections. We have also used semitransparent gold films, instead of ITO, as anode materials and found similar spectral responses at room temperature.

B. Device characterization

The substrates were mounted in a continuous-flow cryostat (Oxford Instruments CF 1204) and kept under vacuum overnight before spectra were taken. Temperature-dependent absorption and photocurrent spectra were measured to temperatures as low as 20 K, monitored by a calibrated RhFe resistance thermometer mounted on the copper sample holder, next to the device. Using an HP4192A impedance analyzer, each of the pixels was tested for short circuits, and their capacitances and conductances compared, as a function of frequency.

For the photocurrent spectroscopy, a 250 W tungsten lamp served as a source of white light, which passed through a Spex 1680B double monochromator, before being focused onto the entrance window of the cryostat. In our experiments, we used a pair of blazed gratings, ruled with 1200 lines/mm, together with appropriate long-pass filters to cover the spectral range 2.75–1.1 eV. For the steady-state (dc) photocurrent spectra, we used a Keithley 237 Source/Measure Unit to apply a fixed bias and measure the current. Typically, after each advance of the monochromator, we waited for 15 s, then took several readings of the current, and averaged these to reduce noise. By taking several averages and advancing in small wavelength steps, we checked that the photocurrent had stabilized and that it was representative of the instantaneous excitation wavelength, rather than being due to photocarriers from earlier (longer) wavelengths which have not decayed. For the modulated (ac) photocurrent spectra, the light was chopped by a mechanical chopper, whose reference signal was fed to the lock-in amplifier, with detection at the chop frequency. We used a feedback circuit to control a steady current source through the polymer light-emitting diode, and measured the voltage modulation across a shunt resistor in series with the polymer diode, which was then amplified and fed to the input of a Stanford SR 530 lock-in amplifier, referenced to the chop frequency. Since we used a differential spectroscopy, we investigated the frequency dependence of the spectral features. The phase information is also used to identify features which share a common origin, and to resolve overlapping features. The excitation spectra which we obtained by the two methods are in excellent agreement.

III. SPECTRAL RESPONSE

For many organic semiconductors, the relationship between the photocurrent and absorption spectra can be classified as one of two types: If they correlate well, so that the maximum photocurrent is obtained for the most strongly absorbed light, the photocurrent response is said to be symbatic with the absorption spectrum. Under other conditions, they are almost complementary; the maxima of the photocurrent action spectrum occur for photon energies where the absorption is weakest, and the photocurrent response is said to be antibatic.

For each diode, we observe both types of photocurrent

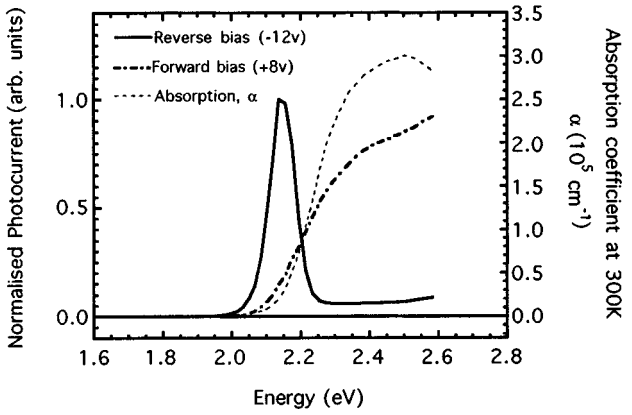

FIG. 2. Photocurrent action spectra at room temperature for the thick diode (ITO/780-nm MEH-PPV/A1) under illumination through the ITO electrode, under forward bias (- · -) and reverse bias (——), with the room-temperature absorption spectrum (- - - -) shown for comparison.

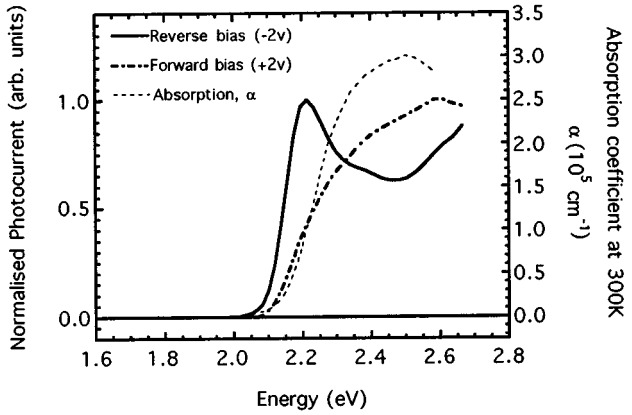

FIG. 3. Photocurrent action spectra at room temperature for the thin diode (ITO/120-nm MEH-PPV/A1) under illumination through the ITO electrode, under forward bias (- · -) and reverse bias (——), with the room-temperature absorption spectrum (- - - -) shown for comparison.

action spectra, depending on the applied bias voltage and the electrode through which it is illuminated. Figure 2 shows both the symbatic and antibatic photocurrent responses for MEH-PPV, obtained for illumination through ITO, under forward bias and reverse bias, respectively. These two distinct contributions differ in their spectral position (energy), line shape and linewidth, bias dependence, frequency dependence, and polarity. We also observed similar features in unsubstituted PPV, albeit shifted to higher energy, due to its higher energy gap; the narrow antibatic photocurrent peaks appears at 2.48 eV, in good agreement with the sharp rise of the photocurrent onset observed by other researchers.[17–23]

Some reports on the photocurrent action spectra do not show such clearly resolved symbatic and antibatic contributions, partly because of different sample geometries, or the use of a higher scan rate when collecting spectra. This can be understood because of the low charge-carrier mobilities of these materials. From impedance spectroscopy of these diodes,[28] we have previously measured *RC* time constants for charging and discharging of the order of milliseconds, and the effects of photoexcitation can persist over rather long time scales, as demonstrated by the slow decay[28] of the low-frequency capacitance or photovoltage back to its dark value, only several minutes or even hours after photoexcitation has ceased. Our modulated photocurrent measurements eliminate this slow decay and are in excellent agreement with steady-state (dc) photocurrent spectra which have been taken sufficiently slowly and under forward or reverse bias. We present the dc photocurrent spectra in the cases where the impedance of the device changes drastically with temperature or applied bias. It should be noted that when the applied bias is small or zero, it is possible to observe both symbatic and antibatic contributions.

Figures 2–5 show the photocurrent action spectra, normalized to an equal photon flux at each energy, with the absorption coefficient of MEH-PPV for comparison. The response is shown for both forward and reverse bias, for two diodes of different thickness.

Figure 2 shows the response of the thicker diode (the 780-nm-thick MEH-PPV layer) to illumination through the ITO electrode. Under forward bias, the photocurrent follows the absorption spectrum (*symbatic* response), while under reverse bias the photocurrent consists of a narrow peak in the low energy tail of the absorption spectrum, which falls away rapidly as the absorption coefficient rises (*antibatic* response). Figure 3 shows a similar behavior for the thinner diode (120-nm-thick MEH-PPV layer), although, under reverse bias, the decrease of the photocurrent in the region of high absorption is not so pronounced, since the film is thinner and self-absorption within the polymer film is therefore reduced.

Figure 4 shows the response of the thicker diode (780-nm MEH-PPV) under illumination through the Al electrode. Figure 5 shows a similar behavior for the thinner diode (120-nm MEH-PPV), except that the responses are broader since the film is thinner, and self-absorption is reduced. For illumination through the Al, the bias dependence is the reverse of that for illumination through ITO (Figs. 2 and 3); the antibatic response occurs under forward bias, while the predominantly symbatic response occurs under reverse bias.

We obtained a linear dependence on light intensity for

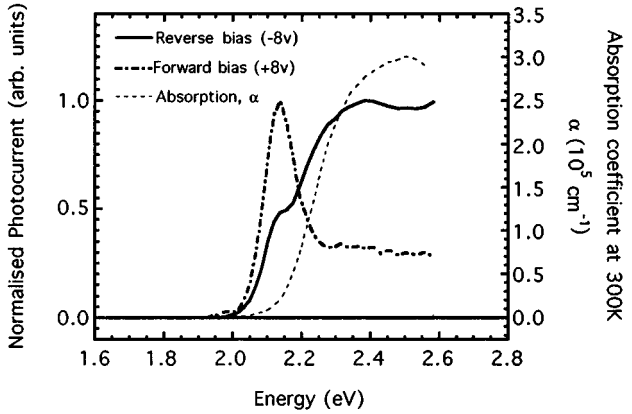

FIG. 4. Photocurrent action spectra at room temperature for the thick diode (ITO/780-nm MEH-PPV/A1) under illumination through the Al electrode, under forward bias (- · -) and reverse bias (——), with the room-temperature absorption spectrum (- - - -) shown for comparison.

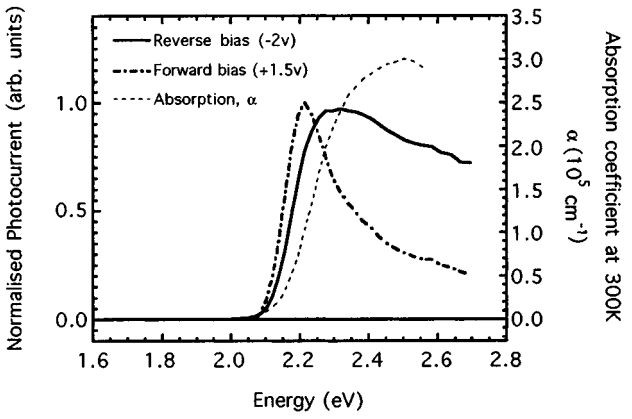

FIG. 5. Photocurrent action spectra at room temperature for the thick diode (ITO/120-nm MEH-PPV/A1) under illumination through the Al electrode, under forward bias (- · -) and reverse bias (——), with the room-temperature absorption spectrum (- - - -) shown for comparison.

over three decades, up to power densities of up to 0.2 μW/pixel for both dc and modulated photocurrents, for both symbatic and antibatic responses, as shown in Fig. 6. The coefficients are 1.01 ± 0.10 for the antibatic peak at 2.16 eV, and 0.93 ± 0.10 for the symbatic peak at 2.26 eV. We also observe linear intensity dependence for single-layer ITO/PPV/Al diodes for both symbatic and antibatic responses. One explanation for the observation of the antibatic peak in the low-energy tail of the absorption spectrum[29] is that, at higher energies, the penetration depth is reduced, so that absorption produces a high density of charge carriers or excitons within a narrow penetration depth, and that these undergo more rapid recombination, resulting in reduced photocurrent yield. We do not consider that bimolecular recombination offers a satisfactory explanation for the antibatic peak in our devices.

Our bias-dependent photocurrent spectra are consistent with the results reported by Marks *et al.*[22] and the following qualitative interpretations: (1) The photocurrent is predominantly due to *p*-type carriers traversing the film. (2) Photoconductivity is an extrinsic process in which carriers are generated by exciton dissociation at whichever electrode offers the shortest drift length for the less mobile photogenerated electron. (3) When the device is biased such that a hole current can only be produced from excitons which dissociate at the far electrode, self-absorption by the intervening polymer film gives rise to an antibatic response (the internal filter effect).

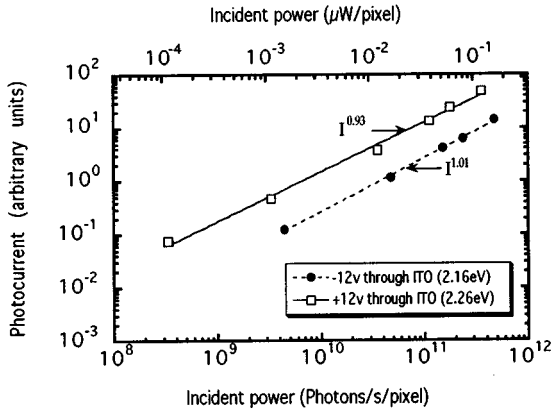

FIG. 6. Dependence of the photocurrent on incident light intensity, showing a linear response for both symbatic and antibatic components.

However, for the thicker diode (780-nm MEH-PPV), shown in Figs. 2 and 4, the antisymmetry between the spectra is not perfect; in Fig. 4, when the device is illuminated through the aluminum electrode, under reverse bias, there is a pronounced shoulder at 2.15 eV, in addition to the otherwise symbatic response. There are two interesting points to note. First, the energy of the shoulder coincides with the energy of the narrow low-energy peak observed under forward bias. Second, the shoulder is absent from the symbatic response observed upon illumination through the ITO electrode, under forward bias (Fig. 2). Furthermore, the low-temperature photocurrent spectra and the following simulations indicate that there may be a specific enhancement at low energy of the quantum efficiency for charge generation. We discuss physical origins for this behavior later, but now consider some of the established models which have been developed to explain the photocurrent response.

IV. MODELING THE PHOTOCURRENT ACTION SPECTRUM

A. Background

It is clear from Figs. 2–5 that self-absorption within the film can partially explain the antibatic behavior. This is sometimes known as the internal filter effect. Several theoretical models have already been developed on this basis, to relate the photocurrent response to the absorption spectrum, assuming an exponential decay of the incident irradiation with distance. However, their assumptions differ, regarding the nature of the initially photoexcited species and the mechanisms of charge generation and transport. In this paper, we consider models developed by Ghosh *et al.*,[30] Tang and Albrecht,[31] DeVore,[32] Ghosh and Feng,[33] and Désormeaux *et al.*[34] These fall into two categories.

In the first category, those of Ghosh *et al.* and Tang and Albrecht consider that carrier generation is only successful within a narrow photoactive region close to one of the electrodes, which henceforth we refer to as the barrier region. Regarding the nature of the barrier, our impedance spectra[28] suggest that it is perhaps not a true Schottky barrier but rather a thin barrier region of fixed width ≈ 10 nm, consisting of metal-oxide layers and insulating, defective regions of the polymer in which oxygen is bonded at or across the vinylene bond.[35–37] In either case, we have seen evidence of a thin, highly resistive layer, across which a high proportion of the applied bias or built-in potential would be dropped, resulting in a high local electric field at the barrier, which could assist exciton dissociation.

In the second category are the models, such as those of DeVore,[32] Ghosh and Feng,[33] and Désormeaux *et al*,[34] which explicitly solve the diffusion equation, either for excitons or free charges, subject to various boundary conditions.

TABLE I. Models for photocurrent action spectra. Comparison of underlying principles.

Model	Method	Species	Boundary conditions	Comments
Ghosh *et al.* (1974)	Narrow zone for generation of carriers	Free charges or excitons	Photocurrent only if minority carrier or exciton reaches barrier layer Generation in barrier layer: $p=1$ Generation in bulk: $p=\exp[-\beta(l-l_b-x)]$	Photocurrent due to all species generated in barrier plus fraction of species from the bulk that can diffuse to barrier layer
Tang and Albrecht (1975)	Narrow zone for generation of carriers	Free charges or excitons	Photocurrent only if minority carrier or exciton generated in barrier layer. Generation in barrier layer: $p=1$ Generation in bulk: $p=0$	No bulk diffusion contribution. Photocurrent due only to species photoexcited within barrier layer Effectively, diffusion length $(1/\beta)\rightarrow 0$
DeVore	Solve diffusion equation	Free charges	Surface recombination currents $(i_R)_0=-D(dn/dx)_{x=0}=-n_0S$ $(i_R)=-D(dn/dx)_{x=l}=n_lS$	Modified to sandwich geometry $J_{\rm ph}(\alpha)\propto 1\Big/\int_0^l \frac{1}{n(\alpha,x)}dx$
Ghosh and Feng (1978)	Solve diffusion equation	Excitons	Exciton density is zero at electrodes $n=0$ at $x=0$ and at $x=l$	Photocurrent due to gradient of exciton density at electrode $J_{\rm ph}\propto -D\left(\frac{dn}{dx}\right)_{x=0}$ or $D\left(\frac{dn}{dx}\right)_{x=l}$
Désormeaux, Max, and Leblanc	Solve diffusion equation, Narrow zone for generation of carriers	Excitons	Exciton density at electrode not zero Rate of generation of carriers within barrier proportional to absorbed light $\dot{n}=\theta I_0\alpha\ \exp[-\alpha x]$ or $\dot{n}=\theta I_0\alpha\ \exp[-\alpha(l-x)]$	Photocurrent due to both: exciton gradient at barrier plus exciton density in barrier layer $J_{\rm ph}\propto -D\left(\frac{dn}{dx}\right)_{x=l_b}+\int_0^{l_b}\dot{n}\ dx$

Further details of all of the models are given in the Appendix. Table I allows a comparison of the assumptions used in these models. The formulas for the predicted spectral dependence of photocurrent are collected in Table II. Although in a qualitative sense, all of these models offer an intuitively reasonable description of the experimental results at room temperature, there are obvious discrepancies which occur when we attempt to use them to quantitatively fit our data to these models.

B. Comparison between experimental and simulated action spectra

In Figs. 7–11, we compare the experimentally observed response for a 780-nm-thick ITO/MEH-PPV/Al sandwich cell under illumination through the ITO electrode, under a reverse bias of -12 V (antibatic response) and under a forward bias of $+12$ V (symbatic response) with the best fits which can be simulated by the various models, namely, those of Ghosh *et al.* (Fig. 7), Tang and Albrecht (Fig. 8), DeVore (Fig. 9), Ghosh and Feng (1978) (Fig. 10) and Désormeaux *et al.* (Fig. 11). Note that, although the models are based on different assumptions, as outlined in Table I, and predict formulas of varying complexity (Table II), the optimized curve fits are all very similar, so that it is difficult to determine which of these models gives the best fit to the data. Furthermore, for the narrow antibatic peak at ~ 2.15 eV, all of the models predict a much broader response, with a much more gradual onset of photocurrent at low photon energies than that which is experimentally observed in this work and in other publications.[17–23] This discrepancy is even apparent in the original paper of DeVore, in which there is a discrepancy between the experimental photocurrent spectrum of antimony sulphide (Sb_2S_3) and that predicted by theory. DeVore makes the comment that there may be electronic transitions which appear in the absorption spectrum and yet give rise to negligible photocurrent. Conversely, we note that there may also be transitions (such as those of charge-transfer excitons) which are not readily apparent in the absorption spectrum but which can be particularly effective in photogeneration of charges. Lee, Yu, and Heeger[21] used the original DeVore model to explain the photoconductivity response of PPV for a film of thickness 300 nm, in a surface cell configuration with two parallel gold strip electrodes, separated by 0.2 mm, rather than the sandwich geometry which we used. Their photocurrent response consists of a sharp onset of photocurrent, followed by a gradual decrease

TABLE II. Models for the photocurrent action spectra. Formulas.

Model	Antibatic response (narrow peak at low absorption)	Symbatic response (broad response, high absorption)
Ghosh *et al.* (1974)	$J_{ph} \propto \int_0^{l-l_b} \theta I_0 \alpha e^{(-\alpha x)} e^{-\beta[l-l_b-x]} dx$ (bulk) $+ \int_{l-l_b}^{l} \theta I_0 \alpha e^{(-\alpha x)} 1 dx$ (barrier)	$J_{ph} \propto \int_{l_b}^{l} \theta I_0 \alpha e^{(-\alpha x)} e^{-\beta[x-l_b]} dx$ (bulk) $+ \int_0^{l_b} \theta I_0 \alpha e^{(-\alpha x)} 1 dx$ (barrier)
Tang and Albrecht (1975)	$J_{ph} \propto \int_{l-l_b}^{l} \theta I_0 \alpha e^{(-\alpha x)} 1 dx$ (barrier only)	$J_{ph} \propto \int_0^{l_b} \theta I_0 \alpha e^{(-\alpha x)} 1 dx$ (barrier only)
DeVore	$n(x) = \frac{\theta I_0 \alpha}{D(\beta^2-\alpha^2)} \left[\exp(-\alpha x) + \left\{ \frac{(S-\alpha D)(D\beta-S)\exp(-\alpha l) + (S+\alpha D)(D\beta+S)\exp(\beta l)}{(D\beta-S)^2 \exp(-\beta l) - (D\beta+S)^2 \exp(\beta l)} \right\} \exp(-\beta x) + \left\{ \frac{(S-\alpha D)(D\beta+S)\exp(-\alpha l) + (S+\alpha D)(D\beta-S)\exp(-\beta l)}{(D\beta-S)^2 \exp(-\beta l) - (D\beta+S)^2 \exp(\beta l)} \right\} \exp(\beta x) \right]$ $J_{ph} \propto 1 \Big/ \int_0^l \frac{1}{n(\alpha,x)} dx$ for a sandwich cell geometry	
Ghosh and Feng (1978)	$J_{ph} \propto \left\{ \frac{2\beta - e^{-\alpha l}[\beta e^{-\beta l} + \beta e^{\beta l} - \alpha e^{-\beta l} + \alpha e^{\beta l}]}{[e^{-\beta l} - e^{\beta l}]} \right\} \times \left\{ \frac{\alpha \theta I_0 D}{(\beta^2-\alpha^2)} \right\}$	$J_{ph} \propto \left\{ \frac{\beta[e^{\beta l} - e^{-\alpha l}] + \beta[e^{-\beta l} - e^{-\alpha l}] + \alpha[e^{-\beta l} - e^{\beta l}]}{[e^{-\beta l} - e^{\beta l}]} \right\} \times \left\{ \frac{\alpha \theta I_0 D}{(\beta^2-\alpha^2)} \right\}$
Désormeaux, Max, and Leblanc	$J_{ph} \propto \frac{\alpha \theta I_0 \beta e^{-\alpha l_b}}{(\beta^2-\alpha^2)} \left[\frac{1 - e^{-\beta(l-l_b)}[2e^{-\alpha(l-l_b)} - e^{-\beta(l-l_b)}]}{[1 - e^{-2\beta(l-l_b)}]} \right] + \theta I_0 \left[1 - \frac{\beta^2 e^{-\alpha l_b}}{(\beta^2-\alpha^2)} \right]$	$J_{ph} \propto \frac{\alpha \theta I_0 \beta e^{-\alpha(l-l_b)}}{(\beta^2-\alpha^2)} \times \left[\frac{1 - e^{-\beta(l-l_b)}[2e^{-\alpha(l-l_b)} - e^{-\beta(l-l_b)}]}{[1 - e^{-2\beta(l-l_b)}]} \right] - \theta I_0 e^{-\alpha l} \left[1 - \frac{\beta^2 e^{\alpha l_b}}{(\beta^2-\alpha^2)} \right]$

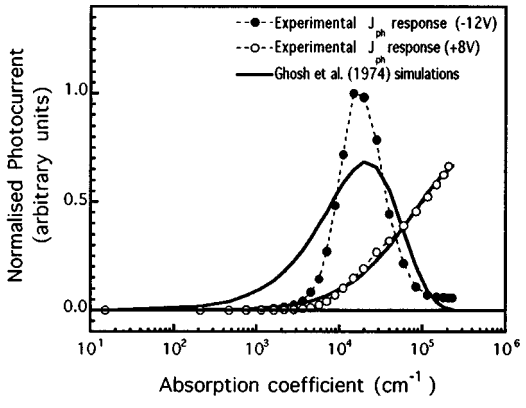

FIG. 7. Comparison of the experimental photocurrent action spectrum (780-nm MEH-PPV) under illumination through ITO under forward bias (- - ○ - -) and reverse bias (- - ● - -), with the responses simulated using the model of Ghosh *et al.* (——).

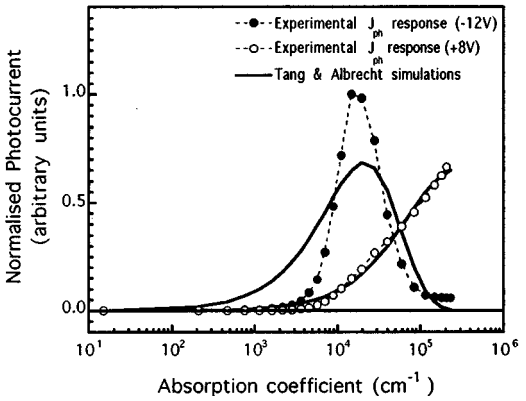

FIG. 8. Comparison of the experimental photocurrent action spectrum (780-nm MEH-PPV) under illumination through ITO under forward bias (- - ○ - -) and reverse bias (- - ● - -), with the responses simulated using the model of Tang and Albrecht (——).

at higher photon energies. This is quite typical for a relatively thin film and for the surface cell geometry. The DeVore model gives a good fit to their experimental data for energies above the peak in the photocurrent, although there is a significant discrepancy at lower photon energies; the experimental data fall below the theoretical curve, just as we find when we apply the DeVore model to our sandwich cells with MEH-PPV. Lee, Yu, and Heeger make a number of arguments in support of the semiconductor band model, which we address in Sec. VIII.

It is also unclear how sensitive the models are to parameters such as the diffusion length of excitons or charge carriers or the thickness of the narrow photoactive barrier layer; the simulation using the model of Ghosh *et al.* is very similar to that obtained using the model of Tang and Albrecht [where the diffusion length $(1/\beta)$ tends to zero], or the model of Ghosh and Feng, where the width of the barrier is no longer an explicit parameter.

V. DEPENDENCE ON AMBIENT ATMOSPHERE

Since the models predict very similar photocurrent responses, it is extremely difficult to use such poor fits to distinguish between whether charge carriers are generated directly as a result of photoexcitation (intrinsic photogeneration), or indirectly (extrinsic photogeneration) by interaction of photoexcited excitons with impurities, defects, traps, and interfaces. The dependence of the photocurrent on the ambient atmosphere offers a way to distinguish between intrinsic and extrinsic photoconductivity.

For many conjugated polymers, molecular oxygen is known to behave as an electron acceptor, resulting in *p*-type doping. If charges were directly photogenerated by an intrinsic process, the doping by molecular oxygen should result in a change of both the photocurrent and the dark current by approximately equal factors. Conversely, if the photogeneration process is extrinsic in origin, then the additional step of dissociation of photogenerated excitons may be sensitive to oxygen, and the photocurrent may be enhanced by a much greater factor than the dark current. Enhancement of the photocurrent in air has been observed in anthracene,[38,39] Langmuir–Blodgett films of polymers with triphenylene side chains,[40] poly(phenylenevinylene),[17] poly(diheptyloxyphenylenevinylene),[41] and other alkoxy-substituted PPV derivatives, including MEH-PPV.[42]

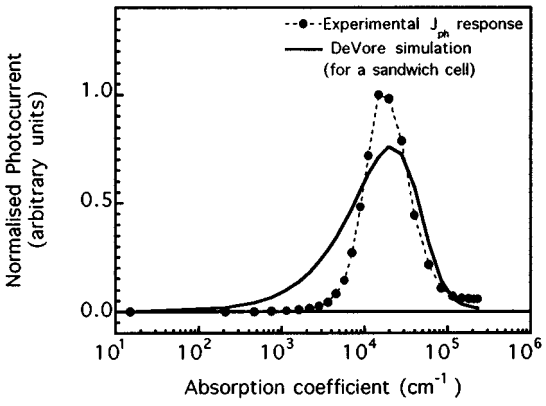

FIG. 9. Comparison of the experimental photocurrent action spectrum (780-nm MEH-PPV) under reverse bias and illumination through ITO (- - ● - -), with the response simulated using the DeVore model modified to a sandwich geometry (——).

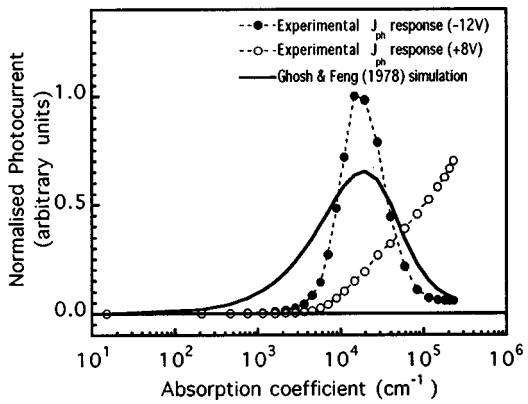

FIG. 10. Comparison of the experimental photocurrent action spectrum (780-nm MEH-PPV) under illumination through ITO under forward bias (- - ○ - -) and reverse bias (- - ● - -), with the responses simulated using the model of Ghosh and Feng (——).

Under reverse bias and illumination through Al, the maximum photocurrent appears for energies greater than 2.3 eV, indicating that the maximum response originates from strongly absorbed light close to the Al electrode. We have observed[27] that the addition of air results in an enhancement of the photocurrent at 2.5 eV by a factor of 6, while the dark current (measured at 1.93 eV) increases by a factor of 1.2. Also, the peak in the action spectrum shifts to higher energy (2.5 eV) closer to the maximum of the absorption coefficient, indicating that the most strongly absorbed light, closest to the Al electrode, is most enhanced by the air.

Under forward bias and illumination through Al, the peak in the photocurrent spectrum occurs at lower energy (2.15 eV). In this case, the photocurrent is greatest from the weakly absorbed light, i.e., that which can reach the ITO electrode. The enhancement due to air is only slight, perhaps

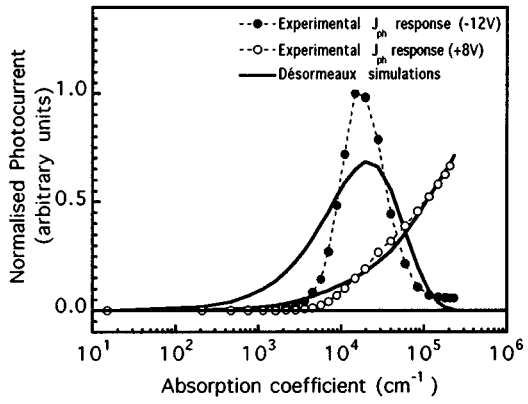

FIG. 11. Comparison of the experimental photocurrent spectrum (780-nm MEH-PPV) under illumination through ITO under forward bias (- - ○ - -), and reverse bias (- - ● - -), with the responses simulated using the model of Désormeaux, Max, and Leblanc (——), without including multiple reflections. (Inclusion of multiple reflections actually resulted in a poorer fit.)

because the gas cannot permeate so deep into the polymer film.

Under reverse bias and illumination through ITO, the peak in the photocurrent spectrum occurs at lower energy (2.15 eV). Now the maximum photocurrent comes from weakly absorbed light, i.e., that which can reach the Al electrode. Upon exposure to air, the photocurrent is enhanced by a factor of 7.1, while the dark current is enhanced by a factor of 1.1.

Under forward bias and illumination through ITO, the peak in the photocurrent spectrum occurs at higher energy (2.26 eV). The maximum photocurrent is due to strongly absorbed light, i.e., photoexcitation close to the ITO electrode. In this case, the admission of air actually results in a decrease of the photocurrent to 0.63 of its value under vacuum.

The consistent picture which emerges from these observations is that the addition of air results in increased photocurrent when the response originates from absorption of light at the Al electrode, while the dark current does not increase significantly. We propose that the charge generation process is extrinsic in nature, and that dissociation of excitons is enhanced by admission of air. The exact mechanism by which air enhances dissociation is uncertain. Oxygen may act as a trap for electrons, providing a low-lying state into which the electron of a bound electron-hole pair may fall; if the energy released by this process exceeds the exciton binding energy, then the exciton can dissociate, releasing a free hole polaron (majority carrier).

It is not clear whether the enhancement due to air is reversible. Although adsorption of air appears to be fairly rapid at the surface, desorption appears to be extremely slow at room temperature, under the reduced pressure of 10^{-6}-torr vacuum within our cryostat, requiring at least 18 h to dedope. Frankevich *et al.*[41] attribute the quasipersistent photoconductivity of poly(diheptyloxy-phenylenevinylene) in air to a very long time delay before positive polarons recombine with O_2^- ions. Antoniadis *et al.*[43] reported increased photoconductivity as a result of creating photo-oxidation defects, mainly carbonyl groups, which act as dissociation centers for excitons. However, Köhler[42] observed that for alkoxy-substituted PPVs, the enhanced photocurrent in the presence of air is reversible if the device is heated under vacuum to assist desorption. In view of this, we consider that the enhanced photocurrent which we observe may not be due solely to photo-oxidation. It is also possible that water vapor (moisture) may play a role in exciton dissociation.

VI. FIELD DEPENDENCE

Under low fields, the photocurrent varies approximately linearly with the applied field, although the dependence is superlinear for higher fields, beginning at fields of the order of 10^5 V/cm. Analysis of the field dependence of the photocurrent and field-induced exciton quenching has been reported by other researchers.[22,29,44–47] From those measurements, the singlet exciton binding energy is estimated to be of the order of 0.4 eV, in agreement with theoretical predictions by Conwell and co-workers,[48,49] and intermediate within the range of published experimental values from around 1 eV (Ref. 50) to around 0.025 eV.[51] Campbell *et al.*[52] estimated a binding energy of 0.2 eV from field-dependent electroabsorption measurements on MEH-PPV. Due to the limited range of our field-dependent photocurrent measurements, an estimate of the exciton binding energy from our data is beyond the scope of this paper.

VII. EXTENSIONS TO THE ORIGINAL MODELS

In Figs. 7–11, we notice that many different models predict very similar profiles, in poor agreement with the experimental response. It is therefore extremely difficult to distinguish between different mechanisms for charge generation and transport in the polymer diodes used in the models, or to extract meaningful values of parameters, such as the barrier width or the exciton diffusion length. We therefore now discuss a number of possible amendments to the original models.

A. Reflection from electrodes

Our initial reaction to the observation of such a narrow peak in the photocurrent spectra under reverse bias was to check whether it was the result of constructive interference of light which had undergone multiple reflections within the polymer film, considering the diode as a Fabry-Pérot étalon. By taking photocurrent action spectra not only at normal incidence but at incidence angles as large as 70° to the substrate normal, and also on diodes having polymer films of various thicknesses, we were able to conclude that constructive interference of light is not the cause of the narrow photocurrent peak, since the peak position did not change on varying the angle of incidence, corresponding to a change of the optical path length within the polymer film by around 12%.

Nevertheless, it is still possible that upon illumination through the transparent ITO electrode, weakly absorbed light which can reach the back electrode (Al) is reflected, leading to a relative increase of the contribution due to the weakly absorbed light, compared to that of the strongly absorbed light, which does not penetrate so far into the film.

Désormeaux, Max, and Leblanc[34] considered the effects of multiple reflections of weakly absorbed light on the photocurrent response of their chlorophyll sandwich cell photodiodes. This was done by using a linear combination of Eqs. (A19) and (A20), with I_0 representing the total light (transmitted and reflected) originating from each electrode, taking into account absorption in the film. Since Eq. (A19) accounts for a symbatic response, while Eq. (A20) produces an antibatic response for sufficiently thick films, the effect of multiple reflection is actually to reduce the ''contrast'' in the action spectrum. This is apparent in the simulated spectra of Désormeaux, Max, and Leblanc (Figs. 5 and 6 of their paper). In our simulations, we cannot improve the fit by inclusion of multiple reflections between the electrodes. In conclusion, we note that although multiple reflections should be included in a comprehensive model for the photocurrent action spectra, they do not account for the particularly narrow photocurrent peak which is experimentally observed but, rather, that they tend to broaden the simulated response by adding a symbatic component to an otherwise antibatic response.

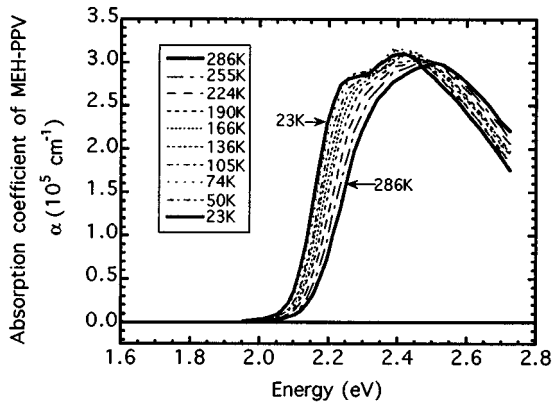

FIG. 12. Temperature dependence of the absorption coefficient of MEH-PPV, showing a progressive redshift and increased vibronic structure at low temperatures.

B. Effects of disorder within polymeric systems

Most of the models discussed in this paper were originally developed for organic semiconductors consisting of small molecules, such as tetracene, phthalocyanines, merocyanines, and chlorophyll. For these materials, the models provide good quantitative agreement with experimental data. However, these systems are much simpler, since the molecules are usually rigid, planar and of well-defined size and conjugation length, i.e., they are essentially monodisperse. Their absorption spectra often consist of several narrow peaks, with clear vibronic structure. Conversely, conjugated polymers generally represent a much more disordered class of material. Most conjugated polymers are polydisperse, i.e., there is a distribution of the molecular weights of the polymer chains. Furthermore, the electronic properties are highly dependent on the *effective* conjugation length, i.e., the length of conjugated segments along which charge is delocalized in the molecular π-electron orbitals. A π-conjugated polymer can be viewed as an assembly of conjugated segments, separated by chemical defects, such as a nonconjugated sp^3-hybridized carbon atom on the polymer backbone, or by structural defects, such as chain kinks or twists out of coplanarity. Hence the polymer can be regarded as a semiconductor material, in which there is a distribution of semiconductor energy gaps. The effect of a change of temperature on the polymer is not merely to activate electronic transitions, but also to change the morphology of the polymer, and hence also to change the distribution of semiconductor energy gaps associated with the material.

C. Thermochromism

Figure 12 shows the temperature-dependent absorption coefficient of MEH-PPV, denoted $\alpha(\hbar\omega)$, which we determined from temperature-dependent absorption spectra of films of four different thicknesses spun on spectrosil discs, to attempt to correct for reflection. At room temperature, the absorption spectrum is broad and almost featureless, with a maximum at 2.50 eV. As the temperature falls, the absorption edge moves progressively to lower energy and, below 150 K, a greater degree of vibronic structure is apparent. At 20 K, two vibronic transitions can be resolved, centered on 2.25 and 2.40 eV. A similar behavior is reported by Lee *et al.*[53] for unsubstituted PPV. Both the progressive redshift of the absorption spectrum and the increasingly apparent vibronic structure at low temperatures can be taken as evidence of an increasingly rigid, less twisted polymer chain and, hence, a general increase in the effective length of conjugated segments, due to a lower density of localized phenylene ring twists, as the thermal fluctuations (k_BT) become progressively small, compared to the torsion potential.

At this point, it is perhaps worthwhile to briefly review the literature on thermochromism in PPV and its alkoxy derivatives. Although several theoretical studies[54–58] on isolated oligo(phenylenevinylene)'s have been undertaken, most predict a rather flat torsion potential with shallow minima for dihedral angles of around 20°, such that solid-state packing effects could easily render the coplanar configuration thermodynamically stable in the solid. This would be in agreement with the experimentally observed redshift of both absorption and fluorescence spectra of oligomers when moving from solution to the solid state. From extrapolation of either the onset of absorption and fluorescence or the 0-0 peaks, effective conjugation lengths have been estimated to be of the order of 7–10 phenylene rings, according to Tian *et al.*[54] and 10–17 rings according to Woo *et al.*[56]

Regarding the effects of alkyl and alkoxy side chains, Lhost and Brédas[55] calculated that the dimer of poly(2,5-dimethylphenylenevinylene) is twisted in the gas phase, due to steric interactions between the methyl groups and the hydrogen atoms on the vinylene bond, resulting in dihedral torsion angles in the range 20°–50°. In contrast, the dimer of poly(2,5-dimethoxyphenylenevinylene) is calculated to be planar, probably due to hydrogen bonding between the oxygen atom of the methoxy substituents and the vinylic hydrogen atoms. These findings are in agreement with crystallographic studies of Martens *et al*,[59] in which poly(2,5-dimethylphenylenevinylene) was found to be disordered, while poly(2,5-dimethoxyphenylenevinylene) is crystalline.

Fahlman *et al.*[58] found excellent agreement between the ultraviolet photoelectron spectra of PPV and its dimethyl and dialkoxy derivatives (including MEH-PPV) and the Austin model 1 and valence effective Hamiltonian quantum-chemical calculations. For PPV, MEH-PPV, and dimethoxy-substituted PPV, they infer an essentially coplanar conformation at room temperature.

Ma *et al.*[60] reported x-ray studies on poly(acetylene) and poly(ethylene), as well as PPV and poly(aniline). For the ring-containing polymers, they concluded that ring-torsion modes are the lowest-energy deformations, and that they are excited at lower temperature than twists of rigid chains, since a smaller mass (i.e., a single phenylene ring) is involved.

Mao *et al.*[61] reported a neutron-diffraction study of all-hydrogen and selectively deuterated PPV, studied from room temperature to 616 K. From structure factor fits, they deduce that, at room temperature, the mean dihedral angle is 7°, with rms angular deviations from this by 6°. Both the mean dihedral angle and the rms deviation from it are found to increase with increasing temperature, due to reduced solid-state packing constraints upon thermal expansion. The torsion is considered to be due to local torsional rotations of phenylene rings, rather than a bulk twist of the whole polymer chain.

Liang and Karasz[62] reported solid-state thermochromism in poly(2-methoxyphenylenevinylene). Up to 300 °C, there is

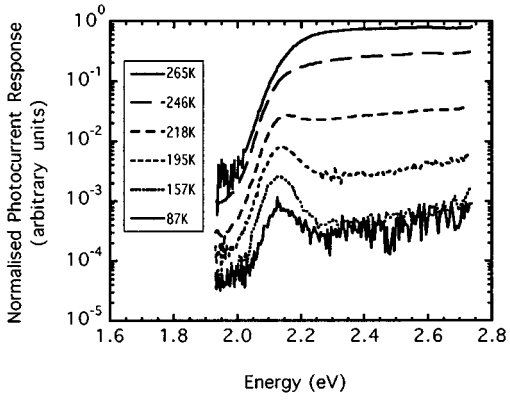

(a)

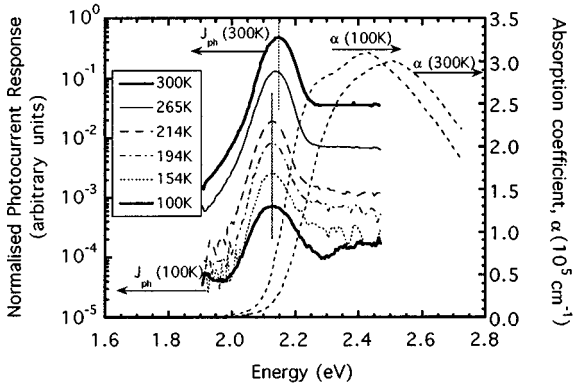

(b)

FIG. 13. Temperature-dependent photocurrent action spectra for the thicker diode (ITO/780-nm MEH-PPV/Al) under illumination through ITO. (a) The photocurrent under forward bias shows the evolution from a symbatic response at room temperature to an antibatic response at low temperature. (b) The photocurrent under reverse bias shows that, as the temperature decreases, the narrow antibatic response undergoes a much smaller redshift than the absorption coefficient over the same temperature range.

a gradual blueshift of the absorption edge with increasing temperature, corresponding to a wagging motion of the rings. Only at 350 °C does a pronounced thermochromic transition occur, which is attributed to 180° ring-flip motion.

The consistent picture which emerges is that the bulk of PPV and MEH-PPV chains are coplanar in the solid state, although local phenylene ring torsions can occur, with very low activation energies, much less than k_BT at room temperature, the mean amplitude and standard deviation increasing with increasing temperature.

There is an important corollary resulting from the thermochromism of poly(phenylenevinylene)'s, which should not be overlooked when attempting to derive activation energies or exciton binding energies from an Arrhenius temperature dependence of the photocurrent; because of the rather sharp onset or absorption, a change in temperature over a small range can result in a remarkably large variation in the amount of self-absorption at a given photon energy in the low-energy region. Therefore great care is needed to correct for this factor when Arrhenius-law plots are used to attempt to determine exciton binding energies and values determined from the temperature dependence of the low-energy photocurrent peak should be treated with great caution. At very

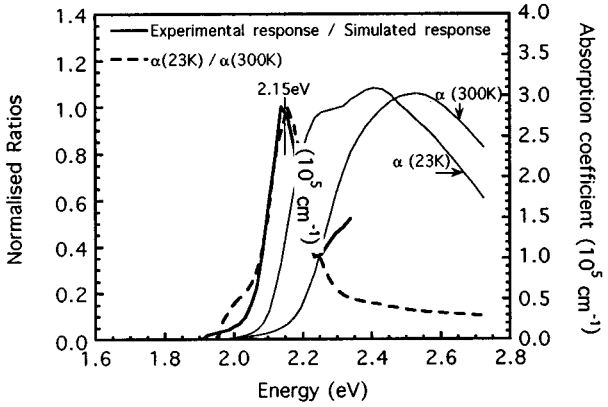

FIG. 14. Investigation of the discrepancy between the simulated and experimental photocurrent action spectra of Fig. 7. The thick solid line (——) is the ratio of the experimental response to the response simulated by the model of Ghosh *et al.* The thick dashed line (- - -) is the ratio of the low temperature absorption coefficient to the room-temperature absorption coefficient of MEH-PPV.

low temperatures, the conductivity of the electrodes may also limit the carrier collection efficiency. For both of these reasons, we consider that studies of the field dependence may be more appropriate for the determination of a binding energy.

D. Temperature dependence of the photocurrent response

The temperature dependence of the photocurrent response is particularly revealing; at temperatures lower than about 200 K, even the symbatic response profile observed for illumination through the ITO electrode under forward bias progressively evolves into the antibatic response located in the low-energy tail of the absorption spectrum, are shown in Fig. 13(a). However, we observe in Fig. 13(b) that the antibatic response undergoes only a very slight redshift upon cooling, typically 0.02 eV, while the redshift of the absorption edge undergoes a much more pronounced redshift ($\Delta E = 0.1$ eV), typically 0.1 eV upon cooling from 300 to 100 K. If the action spectrum were determined solely by the penetration depth of light (the internal filter effect), then, upon cooling, we could expect a redshift of both the antibatic photocurrent peak and absorption edge by the same amount, contrary to what we observe.

E. Modeling the longest chain segments

From the discussion on thermochromism, it seems reasonable to consider that the low-temperature absorption spectrum is representative of the longest, most planar conjugated segments, probably closely packed within crystallite grains. Considering the room-temperature absorption spectrum, it is clear that such long segments account for only a small proportion of all segments which are able to absorb a photon, since the absorption spectrum is dominated by the shorter sections separated by twisted rings. However, we postulate that although all segments may be photoexcited, intermolecular charge separation may be much more efficient when one of the longer planar segments is photoexcited. Possible mechanisms for this are discussed later.

In Fig. 14, we plot the ratio of the experimental response, divided by the optimized simulated photocurrent response,

according to the model of Ghosh *et al.*, as the thick solid line. We also plot the ratio $\alpha_{LT}(\hbar\omega)/\alpha(\hbar\omega, T)$, indicated by the thick dashed line, and note that this gives a qualitatively reasonable trial function for the efficiency of intermolecular charge separation. We considered this ratio for the following reason. For any given photon energy $\hbar\omega$, the number of long, planar segments which are photoexcited will therefore be proportional to the low-temperature absorption coefficient $\alpha_{LT}(\hbar\omega)$, while the total number of segments which are photoexcited will simply be proportional to the absorption coefficient at the ambient temperature $\alpha(\hbar\omega,T)$. We therefore propose to include an energy-dependent function $\theta(\hbar\omega)\propto\alpha_{LT}(\hbar\omega)/\alpha(\hbar\omega,T)$ in our models for the photocurrent action spectra, to represent the interchain splitting probability in place of the constant value of θ used earlier. This trial charge-separation efficiency function shows a pronounced peak at 2.15 eV, which is in good agreement with the energy of the narrow photocurrent peak at low energy. In our brief communication,[27] we compared the experimental data with the model of Ghosh *et al.*, including the extra factor $\alpha_{LT}(\hbar\omega)/\alpha(\hbar\omega,T)$ to represent the longest segments. Inclusion of an energy-dependent function to represent the probability of interchain charge transfer results in a marked enhancement of the photocurrent in the low-energy tail of the absorption spectrum and much better agreement with experimental data.

It is interesting to note that we require enhancement of the photocurrent at low energies to obtain agreement between simulation and experiment. This is in contrast with what is expected if the polymer is highly disordered, and is modeled purely as a statistical distribution of energetic sites, with charge transport mediated by hopping, and no explicit correlation between chain segment length and chain conformation. In that case, it can be argued[45] that the interchain splitting probability may be enhanced for excitation at high energies, since the kinetic energy associated with the exciton is greatest when it is confined to a short chain segment, assuming a simple model of a particle in a one-dimensional box. Hence excitation at high energies should allow greater kinetic energy available for overcoming the Coulomb attraction. Using an average conjugation length of around 7–17 phenylene units, and an absolute minimum spatial extent of a highly confined exciton as 1–2 units, the additional kinetic energy available from confinement may result in an enhancement of up to ten for high photon energies. However, time-resolved studies of photoluminescence decay in PPV, poly(phenylphenylenevinylene) (PPPV) and PPPV/polycarbonate blends by Mollay *et al.*[63] and in PPV and MEH-PPV by Hayes, Samuel, and Phillips[64] indicate that fluorescence from the short high-energy segments decays on a time scale of less than 300 fs, whereas photoluminescence detected at low energies decays on a much slower time scale of around 145 ps, corresponding to emission from the longest segments. A redshift of the luminescence spectra on a time scale of several ps provides strong evidence of exciton diffusion to longer segments of lower energy. However, although the shortest segments no longer contribute to photoluminescence after 300 fs, it is difficult to conclude whether this is due to a greatly enhanced probability of dissociation due to the exciton having a higher kinetic energy, or whether it is due mainly to rapid exciton diffusion to longer segments of lower energy. In any case, the argument concerning kinetic energy does not help to explain an apparent increase in the photocurrent yield at low energy, compared with that predicted by the models based on penetration depth of light.

In the following sections, we discuss possible mechanisms for an enhancement at low energy, corresponding to longer segments. We consider that this may be due to an extended lifetime for localized excitons, or due to enhanced interchain charge transfer or charge transport mediated by π stacking in small crystallites.

VIII. MECHANISMS FOR AN ENHANCEMENT AT LOW ENERGY

A. Energetic disorder, spectral diffusion, and extended lifetime

Within an excitonic picture, a distribution of lengths of the conjugated segments gives rise to the possibility of spectral diffusion of excitons from the shorter segments of relatively high energy to longer segments of lower energy. Once the excitons reside on the longest segments, there are very few sites to which it is energetically favorable for them to diffuse. They have then reached the localization threshold, and we can expect that, at this energy, the exciton diffusion coefficent would be reduced. Hence an exciton on a long segment may have a longer lifetime by up to three orders of magnitude, compared to an exciton at higher energy, as determined by time-resolved photoluminescence decay measurements,[63,64] showing a continuous increase in decay time as emission is probed using progressively lower excitation energy.

We note that for both MEH-PPV and PPV, the position of the narrow antibatic photocurrent peak (2.15 and 2.48 eV, respectively) lies just above the localization energy of excitons[65–67] (2.04 and 2.38 eV, respectively) in MEH-PPV and PPV. We consider that this extended lifetime effect could account for an enhancement of the photocurrent response at low energy under the following two conditions: (1) Exciton dissociation giving rise to photocurrents can only occur for the small fraction of excitons on the longest segments which happen to be situated very near to a dissociation site, such as a metal electrode or an oxygen molecule. (2) Excitons on the longest segments are generated only by direct photoexcitation at low photon energy, and not populated as a result of spectral diffusion of excitons from shorter segments; i.e., although spectral diffusion may operate, the mean separation of the very longest segments exceeds the mean exciton diffusion radius of more energetic short-lived excitons generated on shorter segments.

B. Structural disorder

There may also be intermolecular disorder resulting from structural disorder within the polymer film, which itself may consist of both amorphous and crystalline regions. Karl[68] has noted the importance of structural order on the photoconductivity. Much of the following discussion is based on the ''fringed micelle'' model,[69] which was used to describe the crystalline-amorphous nature of poly(ethene).[70] We consider the possibility of structural inhomogeneity on a length scale of nanometers, and assume that the polymer film consists of

small crystallite grains in addition to amorphous regions, in which the chains are more widely separated. There is evidence for such structural disorder from electron microscopy studies[71–73] of PPV, for which the diameter of crystallite grains is estimated to be in the range 3–12 nm, which is comparable with estimates of the exciton diffusion range.[7,74–76] This can be expected to have a profound effect on charge transport across the film and also on the probability of separation of the geminate positive and negative charges after photoexcitation; charge carriers are more likely to separate and give rise to a photocurrent if one of the charges transfers to a neighboring conjugated segment. Those polymer segments with more extended π conjugation are necessarily more planar, and may be more amenable to effective intermolecular overlap and efficient intermolecular charge transport mediated by π stacking, as is considered to operate in polycrystalline sexithiophene and charge-transfer salts. As we mentioned above, the longer conjugated segments correspond to the lower-energy side of the absorption spectrum. We now consider the possibility of either charge-transfer excitons or enhanced charge transport within crystallites, although the distinction between these two classifications is somewhat blurred.

C. Interchain charge-transfer excitons and aggregation

It has been suggested that charge-transfer excitons are responsible for photoconductivity in both conjugated polymers, and also in the more well-ordered oligomeric systems, such as polycrystalline films of α-sexithiophene.[77] Frankevich *et al.*[78] invoked the concept of interchain polaron pairs to explain an enhancement of the photocurrent in the presence of a magnetic field, in which singlet-triplet crossing is enhanced when the electron-hole pair are sufficiently well separated that the hyperfine interaction exceeds the exchange interaction.

Whereas Frenkel excitons are localized on a single chain and are considered to give rise to luminescence when they decay radiatively, charge-transfer excitons describe electrically neutral photoexcitations which are delocalized over two or more adjacent chain segments. Where these chain segments lie laterally parallel, charge transfer between the chains leads to an electric dipole between the chains. Charge-transfer excitons may be weakly coupled to the ground state, and are not necessarily observed in the linear absorption spectrum. However, they may be observed in electroabsorption spectroscopy, where it is often the case that the response follows the first or second derivative of the absorption spectrum. The position of the narrow antibatic photocurrent response which we observe at 2.15 eV is in close agreement with a peak at 2.15 eV, observed in electroabsorption spectra at MEH-PPV,[50] which has been assigned to a Stark shift of the allowed transition of 1^1B_u exciton at 2.4 eV. The narrow photocurrent peak which we observe at 2.15 eV lies below the energy of either the peak in the first derivative (2.26 eV) or the second derivative (2.20 eV) of the absorption spectrum, although this may be due to self-absorption effects. Except for the smallest applied fields, we observe no continuous shift of the peak position as the magnitude of applied reverse bias field increases, which suggests that the spectral position of the narrow photocurrent peak at 2.15 eV may in fact not be due to a Stark shift. We nevertheless tried to include the derivatives in our models by multiplying by a term proportional to $(d\alpha/dE)/\alpha$ or $(d^2\alpha/dE^2)/\alpha$ to represent excitonic peaks lowered by a Stark shift due to the applied or built-in electric field. However, this approach has not been successful, since the low-energy tail of the absorption spectrum follows an approximately exponential rise with energy, only deviating from this close to the maximum of absorption. Therefore, the absorption coefficient and its derivatives have approximately the same functional form and the term $(d\alpha/dE)/\alpha$ or $(d^2\alpha/dE^2)/\alpha$ reduces to a constant, particularly in the range where the narrow photocurrent peak is observed.

On the basis of a conduction band threshold at 3.5 eV and a large implied binding energy of 1.1 eV, Leng *et al.*[50] considered that the $1B_u$ exciton at 2.4 eV may be an exciton of the charge-transfer type. However, it should be noted that this value of the exciton binding energy is one of the highest values in the literature for PPV and its derivatives. The validity of the assignment to the conduction band threshold of the large increase in photocurrent yield at 3.5 eV has recently been challenged by Köhler *et al.*,[79] since three distinct photocurrent peaks have been observed when measurements are extended far into the ultraviolet.

Yan *et al.* proposed[80] that interchain excitons may play an important role in the nonradiative decay of PPV. The spectral feature which they attribute to spatially indirect interchain excitons is picosecond photoinduced absorption at 1.5 eV, which is in agreement with theoretical calculations by Conwell and Mizes.[49,81,82] The calculated energy of formation of a polaron pair is approximately constant with chain length and it is predicted that polaron pairs should be energetically favored over excitons for chain segments of up to seven monomer units.[49] The long-lived photoinduced absorption is reported not to be observed in dilute solutions of MEH-PPV, and this is taken as evidence[49] that the long-lived photoinduced absorption feature at $\sim$1.5 eV is due to an optical transition within a polaron pair.

There is currently debate about the efficiency of production of interchain excitons versus intrachain excitons. Yan *et al.* suggested[80] that photoexcitation may result in yields of interchain excitons up to 80–90 %. For oligomers, it is well established that close interchain packing in the solid state can result in lower photoluminescence yields compared with well-separated chains in dilute solution.[83] However, the reported estimates of 90% yield of interchain excitons in PPV is apparently in conflict with measurements of photoluminescence quantum efficiencies by Greenham *et al.*,[84] where values of 27% for intrachain singlet excitons are measured for PPV with an initial photoluminescence PL decay time of 320 ps. Studies on deliberately photo-oxidized PPV show reduced photoluminescence yields[75] and increased photoconductivity.[43] In a very recent publication, Rothberg *et al.*[85] proposed that luminescence quenching by carbonyl defects is due to interchain charge transfer; although strong fluorescence is observed for both the PPV trimer, distrylbenzene (DSB) and for *trans*-stilbene-4, 4′-dicarboxaldehyde (SDA), representing a PPV dimer segment terminated by carbonyl groups in place of vinylene bonds, the luminescence from a film of DSB contaminated with 0.6% SDA is essentially quenched. Since DSB and SDA have similar

HOMO-LUMO (highest occupied molecular orbital–lowest unoccupied molecular orbital) gaps, but with an offset of the LUMO levels by 0.59 eV, determined by electrochemical methods, Rothberg *et al.* proposed that, in this case, PL quenching is due to electron transfer from the DSB to the lower-lying SDA, resulting in a nonemissive interchain charge-transfer exciton. However, when DSB is contaminated with the dialdehyde of the trimer, having a lower HOMO-LUMO gap, both electron and hole can transfer to the lower gap material; i.e., energy transfer can occur, with PL emission characteristic of the trimer dialdehyde for the contaminated DSB/trimer dialdehyde film. Hence, the relatively high interchain exciton yield reported by Yan *et al.* may be explained by a difference in the proportion of short photo-oxidized segments between the PPV films, perhaps due to slightly different protocols for synthesis, film preparation, or thermal conversion from the precursor polymer.

In any case, we note that the characteristic transition energy ($\sim$1.5 eV) of the interchain polaron pair is well below the energy of the singlet exciton responsible for fluorescence, so that while electron transfer or energy transfer from the singlet exciton to an interchain exciton may occur, it is not obvious that it should account for a specific enhancement of the photocurrent yield upon excitation at the low-energy tail of the absorption edge. Furthermore, the calculations of Conwell and Mizes and the recent investigations on oligomers both indicate that formation of polaron pairs should be most favorable for excitons residing on the shortest chain segments, i.e., excited at higher photon energies.

Aggregation of ladder-type poly(paraphenylene) is observed in the solid state,[86,87] characterized by a broad featureless emission band in PL and electroluminescence at lower energy than the narrow, structured emission from the isolated chains. Köhler *et al.*[88] investigated the photovoltaic response of these materials, and observed a much greater quantum efficiency for photocarrier generation when the aggregate band is excited directly. Gelinck, Warman, and Staring recently reported higher microwave conductivity for the gel form of an alkoxy-substituted PPV derivative, compared to the value in solution. The implication is that charge separation is enhanced in aggregated chains in the gel form. Broad featureless emission spectra are observed for cyano-substituted derivatives of MEH-PPV and poly(dihexyloxyphenylenevinylene) and are attributed to excimer emission.[67] Conversely, the PL spectra of PPV and MEH-PPV show clear vibronic structure, and it is generally observed that aggregation and interchain effects are not so apparent in these materials, in spite of the high degree of crystallinity for PPV in the solid state.[59] Even if some singlet excitons do undergo interchain charge-transfer leading to generation of unbound polaron charge carriers, the quantum yield for photocarrier generation in single-layer devices ($\sim$1% according to Marks *et al*[22]) is so much lower than the quantum yield for photoluminescence that it would be difficult to observe as a strongly competing non-radiative decay channel.

D. Enhanced interchain transport within crystallites

Even if aggregation effects are not so pronounced as to be apparent as a broad featureless emission band in the photoluminescence of MEH-PPV and PPV, it may still be the case that, within crystallites, the interchain separation is sufficiently small for markedly enhanced interchain transport. Brown *et al.*[90] collated conductivity and mobility data on amorphous conjugated polymers and other organic semiconductors. A universal conductivity-mobility relationship holds for most amorphous conjugated polymers, resulting in poor performance in field-effect transistors; higher mobilities can be achieved only by increasing the doping level, which therefore reduces the on/off current ratio. However, partially crystalline systems, such as α-sexithiophene, exhibit much higher field-effect mobilities together with high on/off current ratios and low doping levels.[91,92] In these materials, charge transport is considered to be greatly enhanced by π stacking, in which charge transport preferentially occurs perpendicular to the length of the molecules, in the interchain (stacking) direction, rather than along the direction of π conjugation (long molecular axis).[91,93] This is in contrast with the interchain hopping mechanisms, which are considered to operate in the amorphous materials, including many conjugated polymers. Considering these two different charge-transport mechanisms at a nanometer scale, it is apparent that during the exciton dissociation event, separation of positive and negative charges may be much easier when the exciton is located in a small crystallite grain than when it is located in a relatively amorphous region. Given the increased mobility within crystalline material by a factor of over 1000 (comparing the field-effect mobilities of crystalline α-6T and its amorphous randomly substituted alkyl side-chain derivative, β,β'-dihexyl-6T),[93] it is possible that the degree of ordering on a nanometer scale may result in a much larger enhancement of the interchain splitting probability than that due to confinement. However, we emphasize that once the exciton dissociation has occurred, charge transport through the bulk of the polymer film is likely to be rate limited by hopping mechanisms, and that the above hypothesis does not invalidate the charge-transport work of Arkhipov *et al.* in any way.

Π stacking is known to be very sensitive to the overlap of π-electron wave functions between chains and interchain separations of less than 0.4 nm are usually required to observe such effects. Large twists of the phenylene ring out of planarity will tend to increase the interchain separation. We therefore consider that the longest, most planar conjugated segments may be most amenable to efficient interchain charge transport. This is consistent with the observations of Takiguchi *et al.*,[19] who reported the photocurrent action spectra of stretched PPV films in a surface cell geometry, under polarized light. For light polarized parallel to the stretching direction, the narrow photocurrent peak is observed in the low-energy side of the absorption spectrum, at an energy of 2.4–2.5 eV. For comparison, we recall that in PPV sandwich cells,[28] we observe similar characteristics to that reported here for MEH-PPV (Fig. 2), but with the narrow antibatic photocurrent peak shifted to 2.48 eV, due to the blue shift of the absorption and emission spectra of PPV. The position of our antibatic peak in PPV is therefore in agreement with the results of Takiguchi *et al.* For light perpendicular to the stretching direction, the response is broader and peaked at higher energy. The data of Takiguchi *et al.* are consistent with our hypothesis that exciton splitting is enhanced for extended, aligned chain segments either by charge transfer or enhanced charge transport, thus accounting for the sharp onset of photoconductivity in the low-energy

tail of absorption. We consider that when attempting to model the photocurrent action spectra of PPV and its partially crystalline derivatives quantitatively, enhanced exciton splitting in crystallites may be as important a factor as self-absorption within the film (internal filter effect).

IX. DISCUSSION

Lee, Yu, and Heeger[21] made a number of arguments in favor of the semiconductor band model and intrinsic photogeneration of free carriers, rather than photogeneration of excitons, which subsequently diffuse to dissociation centers, yielding charge carriers. We now address these issues. From studies of the transient photocurrent peak on the subnanosecond time scale, Lee, Yu, and Heeger remarked that the temperature dependence of the transient photocurrent peak is only thermally activated above 200 K, and appears to be independent of temperature below 200 K. We have observed similar behavior, but discussed the complications in determination of the binding energy from the temperature dependence, because of the progressive redshift of the absorption edge and the untwisting of the chain upon cooling, as well as the strong non-Arrhenius temperature dependence of the dark current (mobility), which we observe.

Regarding the validity of the excitonic picture, Lee, Yu, and Heeger questioned why the photocurrent action spectrum shows structure related to excitonic transitions, while the absorption band of PPV is apparently structureless. This can be understood if we consider the morphology of the polymer chain as an assembly of conjugated segments, delineated by chain twists and kinks. Rather than treating PPV as a semiconductor with a single fixed semiconductor band gap, it is probably more appropriate to treat it as a mixture of oligomeric segments, each with slightly different energy gaps, such that, when taken collectively, the sharp excitonic structure is blurred by convolution of the excitonic spectra with the distribution or π-π^* energy gaps, although we note that spectral structure is apparent in films of well-ordered or aligned chains of PPV, and also at lower temperatures, when polymer chains are more planar and the distribution of conjugation lengths becomes narrower and weighted more heavily toward longer segments.[20]

A further criticism of the applicability of the exciton model is that the reciprocal of the photocurrent should be linearly dependent on the reciprocal of the absorption coefficient, a result noted in the paper of Ghosh and Feng. The fact that PPV does not show a linear relationship does not rule out the exciton model, since the linear relationship can only be expected to hold for a semiconductor with a single energy gap, such as a monodisperse oligomer, rather than for a polymer with a distribution of energy gaps.

The remark by Lee, Yu, and Heeger that, if an excitonic model holds, then the photocurrent response should be similar to the absorption spectrum (symbatic), since more excitons are created near the surface, and that the observation of an antibatic response somehow invalidates the excitonic model clearly ignores the work of Ghosh *et al.*, Tang and Albrecht, and others, none of whom are cited by Lee, Yu, and Heeger but all of whom recognized the possibility of self-absorption within the film (internal filter effect) in explaining an antibatic photocurrent peak of a diode with asymmetric electrodes, when it is illuminated through the side furthest from the electrode at which rectification and exciton dissociation occur.

Finally, we reject the argument that for poly(phenylene vinylene)'s, it is possible to distinguish between semiconductor band models and excitonic models, depending on whether the onset of photocurrent coincides with the onset of absorption, taken as upholding the band model, or whether it occurs at a higher energy than the onset of absorption, due to a perceived need to overcome the exciton binding energy. In reply, we point out that the exciton binding energy need not be supplied optically in our sandwich cells; at the interface with the aluminum electrode, exciton dissociation may occur simply due to a higher electric field in this barrier region, and perhaps also by tunneling of an electron from the bound electron-hole pair into a surface state or even the Fermi level of the aluminum electrode, leaving behind a free hole. We remark that the correlation between the DeVore model and the experimental data is so poor in this critical low-energy region, giving a discrepancy of 0.2 eV in the photocurrent onset between experiment and the DeVore theory, that it is doubtful whether ''the semiconductor band model is fully consistent with the data.''

X. CONCLUSIONS

We have measured photocurrent action spectra in the visible region for MEH-PPV films of various thicknesses, in a sandwich cell geometry between electrodes of ITO and semitransparent aluminum, for various applied biases and directions of incidence. From the large enhancement of the photocurrent but not the dark current upon exposure to air, we infer that photogeneration of charge is an extrinsic process, following dissociation of excitons, either in the presence of oxygen molecules acting as electron traps, or at metal electrodes, into which an exciton may expel an electron. We have compared our results with various established models which relate the photocurrent response and absorption coefficient. The simulated action spectra which we calculate using the various models are all very similar, despite different assumptions being made about whether photoexcitation results in free carriers or excitons, their diffusion coefficients and the width of any barrier layer which might enhance exciton dissociation, so it is not clear that any of these parameters may be extracted with any degree of reliability. Furthermore, the simulations are generally in poor agreement with the experimental data. Although the internal filter effect is an important contributory factor for a qualitative explanation of the symbatic and antibatic responses, our main conclusion is that we can only explain the very sharp rise of the photocurrent at low energy in terms of a specific enhanced probability of intermolecular charge separation for the longest, most planar segments. We consider that possible mechanisms for this enhancement include an extended lifetime for excitons near the localization threshold, or an enhanced interchain charge separation in small crystalline grains within the film, perhaps mediated by π stacking.

ACKNOWLEDGMENTS

One of us (M.G.H.) would like to thank St. John's College, Cambridge for financial support. We also thank A.

D. Yoffe and R. H. Friend for interesting and fruitful discussions, A. B. Holmes and Cambridge Display Technology Ltd. for kindly supplying us with materials, and also C. J. Moss and H. E. Thompson for technical advice and assistance with the amplification and detection of the modulated photocurrent spectra.

APPENDIX: DETAILS OF THE MODELS

1. Introduction

Light is incident on the diode, through one electrode, at $x=0$. The rate of generation of charge carriers in the bulk at distance x from the illuminated electrode is taken to be proportional to the light intensity at x, as in Eq. (A1), in which $\alpha(E)$ is the absorption coefficient of the polymer as a function of photon energy E, I_0 is the incident photon flux density, and θ represents the quantum efficiency of charge generation by light:

$$\frac{dn}{dt}=\theta I_0\alpha\ \exp(-\alpha x). \tag{A1}$$

Most of the models are based on a limited diffusion range of either excitons or charge carriers. Throughout this appendix, τ represents the bulk recombination time of the diffusing species, D the diffusion coefficient, and β the reciprocal of the diffusion length ($\beta=1/\sqrt{D\tau}$).

2. Models based on a narrow photoactive layer (barrier region)

At this stage, the models of Ghosh *et al.* and Tang and Albrecht follow a simpler derivation, as outlined below.

a. The model of Ghosh et al.

In 1974, Ghosh *et al.*[30] developed a model which they applied to magnesium phthalocyanine (MgPh) in a sandwich cell of the structure Ag/MgPh/Al. They considered that, in MgPh, excitons were easily dissociated into free carriers and that the photocurrent action spectrum was determined by diffusion of photogenerated free carriers rather than diffusion of excitons. In one of their earlier publications, on the photocurrent response of tetracene sandwich cell of the structure Au/tetracene/Al, Ghosh and Feng[94] also observed both symbatic and antibatic responses, depending on the direction of illumination and whether the diode was operated under forward or reverse bias. In that paper, they noted the importance of the Al tetracene interface on the carrier generation process, and suggested that it may result in dissociation of excitons at the electrodes. In the original paper, the narrow photoactive region at the electrode was attributed to a Schottky barrier. However, for our diodes with PPV and MEH-PPV, there is little evidence of a change of depletion width with bias. Whatever the nature of the narrow photoactive region, we denote its width as l_b, while the total width of the polymer layer in the sandwich cell diode is denoted as l.

The original assumptions of the model are the following.

(i) Photoexcitation produces either free electrons and holes or at least excitons which immediately form free carriers in the bulk, e.g., by interaction with impurities or traps.

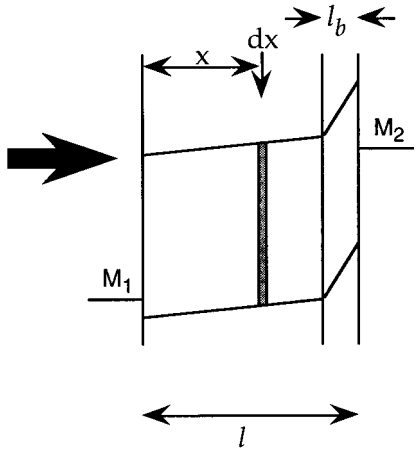

FIG. 15. Schematic device cross section for the model of Ghosh *et al.* (1974) for illumination from the side furthest from the barrier region (i.e., from $x=0$). The total polymer thickness is denoted as l, while the thickness of the barrier layer is denoted l_b, with L the effective diffusion length for carriers.

(ii) The most photosensitive region is the region at the aluminum/MgPh interface.

(iii) The photocurrent depends on the ability of the minority carrier (electrons) to reach the interface, which acts as a sink for them; otherwise, build-up of space-charge will occur within the bulk of the film, impeding charge transport. Therefore, the minority carriers must either be generated in the bulk and subsequently diffuse to the interface or else be generated in the interface region.

However, the model can be applied to either diffusing charge carriers or diffusing excitons. Within the excitonic picture, assumption (iii) is supplemented by the requirement of excitons to reach the aluminum electrode in order to undergo dissociation and produce charge carriers.

(1) Illumination through the electrode far from the barrier. Rearranging Eq. (A1) and referring to Fig. 15, the number of photocarriers produced in range $x\rightarrow x+dx$ from the illuminated surface is given by Eq. (A2),

$$\theta I_0\alpha\ \exp(-\alpha x)dx. \tag{A2}$$

Of the carriers generated at a depth x into the film, the probability of diffusing to the junction is

$$\exp[-\beta(l-l_b-x)]. \tag{A3}$$

Therefore, the total number of carriers n at the junction:

$$n=\int_0^{l-l_b}\theta I_0\alpha\ \exp(-\alpha x)\ \exp[-\beta(l-l_b-x)]dx \quad \text{(bulk)}$$

$$+\int_{l-l_b}^{l}\theta I_0\alpha\ \exp(-\alpha x)1dx \quad \text{(barrier)}. \tag{A4}$$

(2) Illumination through the electrode closest to the barrier. The total number of carriers n at the junction is given by Eq. (A5) (see Fig. 16),

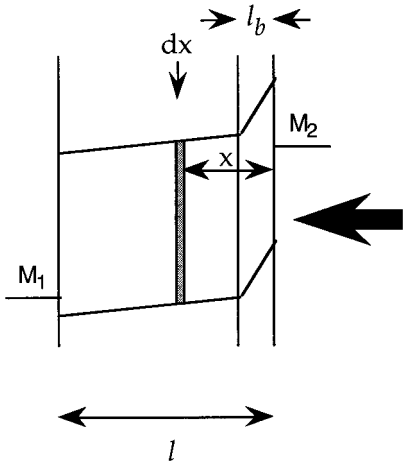

FIG. 16. Schematic device-cross-section for the model of Ghosh *et al.* (1974) for illumination from the side nearest to the barrier region (i.e., from $x=l$). The total polymer thickness is denoted as l, while the thickness of the barrier layer is denoted l_b, with L as the effective diffusion length for carriers.

$$n=\int_0^{l_b}\theta I_0\alpha\,\exp(-\alpha x)dx \quad \text{(barrier)}$$
$$+\int_{l_b}^{l}\theta I_0\alpha\exp(-\alpha x)\exp[-\beta(x-l_b)]dx. \quad \text{(bulk)} \tag{A5}$$

b. The model of Tang and Albrecht

The derivation followed by Tang and Albrecht[31] is essentially a simplified version of that of Ghosh *et al.*, in which the contributions from photoexcitation within the bulk of the film are omitted from Eqs. (A4) and (A5), i.e., neglecting diffusion to the photosensitive barrier layer. Tang and Albrecht also note that for the antibatic response, the curve fits are not particularly sensitive to the width of the barrier.

3. Models based on solution of the diffusion equation

The models of DeVore; Ghosh and Feng (1974); and Désormeaux, Max, and Leblanc all share the same diffusion equations [Eqs. (A6) and (A7)]. Once formed, charge carriers either leave by diffusion or recombination. The rate of change of charge carrier density at a depth x is therefore given by Eq. (A6), in which the first term represents photogeneration, the second term represents carriers moving away by diffusion, while the third term represents recombination of charge carriers on a time scale given by τ, the bulk recombination lifetime:

$$\frac{dn(x)}{dt}=\theta I_0\alpha\,\exp(-\alpha x)-\frac{di}{dx}-\frac{n}{\tau}. \tag{A6}$$

At equilibrium, the charge density does not change with time, so $dn(x)/dt$ is zero. By setting the time derivative $dn(x)/dt$ to zero and recalling that the diffusion current is given by $i=-D\,dn/dx$, where D is the diffusion constant, a time-independent second-order differential equation is obtained for the steady-state distribution of carrier density, as in Eq. (A7);

$$\frac{d^2n(x)}{dx^2}=\frac{n}{D\tau}-\frac{\theta I_0\alpha\,\exp(-\alpha x)}{D}. \tag{A7}$$

Note that in the models of Ghosh and Feng and Désormeaux, Max, and Leblanc, the diffusion equations (A6) and (A7) can also be applied to diffusion of excitons, where $n(x)$ represents the exciton density.

Equation (A7) has the general solution given by Eq. (A8),

$$n(x)=B\,\exp(-\beta x)+C\,\exp(\beta x)+\frac{\theta I_0\alpha\,\exp(-\alpha x)}{D(\beta^2-\alpha^2)} \tag{A8}$$

where $\beta=1/\sqrt{D\tau}$ is the reciprocal of the diffusion length. The values of the coefficients B and C depend on the boundary conditions, which are different for each model, as outlined in Table I.

a. The DeVore model

This model was developed to account for the photoconductivity action spectra of inorganic semiconductors, in which photoexcitation is considered to result directly in the formation of pairs of free electrons and holes. Recombination of electrons and holes can occur in the bulk after a mean lifetime τ or at either surface at a rate which is represented by a recombination current $i_R=n_sS$, where n_s is the density of electron-hole pairs at the surface and S is the surface recombination velocity. When the thickness of the film is comparable with the reciprocal of the maximum value of the absorption coefficient, a high surface recombination velocity S [much greater than the bulk recombination rate, $\beta D=\sqrt{(D/\tau)}$] results in an antibatic response, while a low surface recombination rate gives a symbatic response.

The diffusion equation (A7) is solved subject to the two boundary conditions, given in Eqs. (A9), from which expressions for B and C can be obtained. At the illuminated surface,

$$(i_R)_0=-D(dn/dx)_{x=0}=-n_0S. \tag{A9}$$

At the far surface,

$$(i_R)_l=-D(dn/dx)_{x=l}=-n_lS.$$

The coefficients B and C are then given as in Eq. (10),

$$B=\frac{\theta I_0\alpha/D}{(\beta^2-\alpha^2)}\left\{\frac{(S-\alpha D)(D\beta-S)\,\exp(-\alpha l)+(S+\alpha D)(D\beta+S)\,\exp(\beta l)}{(D\beta-S)^2\,\exp(-\beta l)-(D\beta+S)^2\,\exp(\beta l)}\right\},$$

$$C=\frac{\theta I_0\alpha/D}{(\beta^2-\alpha^2)}\left\{\frac{(S-\alpha D)(D\beta+S)\,\exp(-\alpha l)+(S+\alpha D)(D\beta-S)\,\exp(-\beta l)}{(D\beta-S)^2\,\exp(-\beta l)-(D\beta+S)^2\,\exp(\beta l)}\right\}. \tag{A10}$$

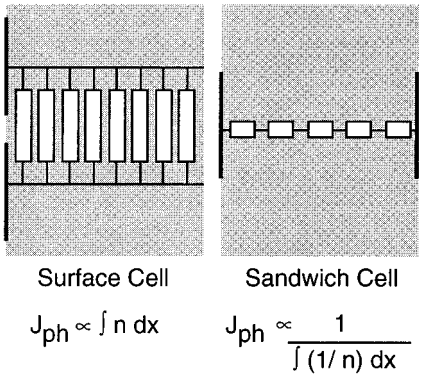

FIG. 17. Conceptual diagram for the modification of the DeVore model to the sandwich geometry, illustrating the need to integrate series resistances for the sandwich cell geometry, rather than parallel conductances, as for the surface cell geometry.

The increase in conductivity is assumed to be proportional to the total number of carrier pairs, i.e., the integral of the carrier density over the length of the film, as in Eq. (A11). This only strictly applies for a surface-cell configuration,

$$N=\int_0^l n(x)dx=\frac{1}{\beta}\{B(1-\exp(-\beta l))+C(\exp(\beta l)-1)\} + \frac{\theta I_0 \alpha/D}{\alpha(\beta^2-\alpha^2)}(1-\exp(-\alpha l)). \tag{A11}$$

The photoconductivity σ_{ph} is then given by the expression $\sigma_{ph}=N/I_0\tau$, and simplifies to the expression given in Eq. (A12), again only valid for a surface cell geometry,

$$\sigma_{ph}=\frac{1-\exp(-\alpha l)}{1+(S/\beta D)\coth(\beta l/2)} \times\left\{1+\frac{(S/\beta D)\beta\,[\beta\coth(\beta l/2)-\alpha\coth(\alpha l/2)]}{\beta^2-\alpha^2}\right\}. \tag{A12}$$

As noted in an appendix of a publication by Gregg, Fox, and Bard,[95] it may not be appropriate to integrate the charge density across the film when calculating the photocurrent action spectrum for a sandwich cell geometry. When mobilities of charge carriers are low, it may in fact be more appropriate to consider the variation of resistance along the thickness of the film, viewed as several resistances arranged in series, the conductivity of the film in a sandwich cell geometry being determined by the most resistive sections, rather than the most conductive. In this case, it is more appropriate to integrate the resistance of each differential length element across the film thickness, rather than integrating the charge density. This point is illustrated in Fig. 17 for clarification.

We have therefore adapted the DeVore theory[32] to a sandwich cell geometry. The method is the same up to the derivation of the charge carrier density [Eqs. (A7)–(A10)]. The photocurrent in the sandwich cell is then proportional to the reciprocal of the integral of the resistivity, as in Eq. (A13), where the carrier density $n(x)$ is that given by Eqs. (A8)–(A10),

$$\sigma_{ph}(\alpha)\propto\frac{1}{\int_0^l\frac{1}{n(\alpha,x)}dx}. \tag{A13}$$

Unfortunately, the expression has no analytical solution, so we performed the integration numerically, dividing the film thickness into 200 steps and optimizing the parameters β, S, and D in order to minimize the sum of squared difference between experimental and simulated profiles. We also performed the numerical integration with 2000 steps, to check that the same profile was obtained.

An antibatic photocurrent response can occur because the photocurrent is limited by the most resistive region, generally that which is furthest away from the illumination. Hence weakly absorbed light can penetrate throughout the film and, assuming intrinsic carrier generation, generate charge carriers throughout the film. Conversely, strongly absorbed light does not penetrate far into the film and, thus, while it can generate a high charge density close to the illuminated electrode, the remainder of the film, beyond a $1/e$ light penetration depth of approximately 30 nm, is much more resistive. Therefore, for relatively thick films, the model predicts a maximum photocurrent peak in the low energy tail of the absorption spectrum.

b. The model of Ghosh and Feng

In a later paper,[33] Ghosh and Feng developed a model which has some initial similarities with the model of DeVore,[32] based on the diffusion of photogenerated species, except that these were again taken to be excitons in merocyanine, just as in tetracene and anthracene, rather than free electrons and holes, as in MgPh. Also, it is important to note that the Ghosh and Feng model was developed for a sandwich cell geometry. The same diffusion equation appears [Eq. (A7)], though subject to slightly different boundary conditions, namely, that the exciton density falls to zero at the electrodes ($n=0$ at $x=0$). Solution of the diffusion equation subject to these boundary conditions yields an expression for the exciton density, as given in Eq. (A14),

$$n=\frac{\alpha\theta I_0}{\beta^2-\alpha^2}\left[\left(\frac{e^{\beta l}-e^{-\alpha l}}{e^{-\beta l}-e^{\beta l}}\right)e^{-\beta x} -\left(\frac{e^{-\beta l}-e^{-\alpha l}}{e^{-\beta l}-e^{\beta l}}\right)e^{\beta x}+e^{-\alpha x}\right], \tag{A14}$$

where $\beta=1/\sqrt{D\tau}$. Furthermore, the photocurrent is taken to be proportional to the gradient of the exciton density at the aluminum electrode, whereas, in the modified DeVore model, the photoconductivity in a surface cell geometry is evaluated by integrating the resistivity over the whole film thickness. For illumination through the aluminum electrode, the photocurrent is given by Eq. (A15), resulting in a symbatic response

$$J_{\mathrm{Al}}=-D\left(\frac{dn}{dx}\right)_{x=0},$$

$$J_{\mathrm{Al}}=\frac{\alpha\theta I_0 D}{(\beta^2-\alpha^2)} \times\left\{\frac{\beta[e^{\beta l}-e^{-\alpha l}]+\beta[e^{-\beta l}-e^{-\alpha l}]+\alpha[e^{-\beta l}-e^{\beta l}]}{[e^{-\beta l}-e^{\beta l}]}\right\}. \tag{A15}$$

For illumination through the silver electrode, the photocurrent is given by Eq. (A16), resulting in an antibatic response for sufficiently thick films,

$$J_{\mathrm{Ag}}=D\left(\frac{dn}{dx}\right)_{x=l},$$

$$J_{\mathrm{Ag}}=\frac{\alpha\theta I_0 D}{(\beta^2-\alpha^2)} \times\left\{\frac{2\beta-e^{-\alpha l}[\beta e^{-\beta l}+\beta e^{\beta l}-\alpha e^{-\beta l}+\alpha e^{\beta l}]}{[e^{-\beta l}-e^{\beta l}]}\right\}. \tag{A16}$$

c. The model of Désormeaux, Max, and Leblanc

The model of Désormeaux, Max, and Leblanc is in fact a hybrid of the two approaches followed by Ghosh *et al.*[30] and Ghosh and Feng,[33] and is applied to sandwich cell photodiodes consisting of Langmuir-Blodgett films of chlorophyll-*a*, chlorophyll-*b*, or a zinc porphyrin derivative between semitransparent silver and aluminum electrodes. It is assumed that charge carriers are generated by dissociation of excitons, mainly at the aluminum interface. The same diffusion equation (A7) is solved, though the boundary conditions are different; the exciton density or carrier density at the aluminum electrode is nonzero and proportional to the integral of the light absorbed within the barrier region, as indicated in Eq. (A17) for light incident through the aluminum electrode and in Eq. (A18) for light incident through the silver electrode, furthest from the barrier,

$$n_{\mathrm{Al}}=\int_0^{l_b}\theta I_0\alpha\,\exp(-\alpha x)dx=\theta I_0[1-\exp(-\alpha l_b)], \tag{A17}$$

$$n_{\mathrm{Ag}}=\int_0^{l_b}\theta I_0\alpha\,\exp[-\alpha(l-x)]dx =\theta I_0\{\exp[-\alpha(l-l_b)]\}[1-\exp(-\alpha l_b)]. \tag{A18}$$

Following the model of Ghosh *et al.*, the photocurrent consists of both bulk and barrier contributions, i.e., a current proportional to the gradient of the carrier density at the barrier and a contribution proportional to the density of carriers directly produced in the barrier region. The model therefore predicts photocurrent responses given by Eq. (A19) for light incident through the aluminum electrode and by Eq. (A20) for light incident through the silver electrode, furthest from the barrier region:

$$J_{\mathrm{Al}}=-D\left(\frac{\partial n}{\partial x}\right)_{l_b}+n_{\mathrm{Al}},$$

$$J_{\mathrm{Al}}=\frac{\alpha\theta I_0\beta e^{-\alpha l_b}}{(\beta^2-\alpha^2)}\left[\frac{1-e^{-\beta(l-l_b)}[2e^{-\alpha(l-l_b)}-e^{-\beta(l-l_b)}]}{[1-e^{-2\beta(l-l_b)}]}\right] +\theta I_0\left[1-\frac{\beta^2 e^{-\alpha l_b}}{(\beta^2-\alpha^2)}\right], \tag{A19}$$

$$J_{\mathrm{Ag}}=-D\left(\frac{\partial n}{\partial x}\right)_{l_b}+n_{\mathrm{Ag}},$$

$$J_{\mathrm{Ag}}=\frac{\alpha\theta I_0\beta e^{-\alpha(l-l_b)}}{(\beta^2-\alpha^2)}\left[\frac{1-e^{-\beta(l-l_b)}[2e^{\alpha(l-l_b)}-e^{-\beta(l-l_b)}]}{[1-e^{-2\beta(l-l_b)}]}\right] -\theta I_0 e^{-\alpha l}\left[1-\frac{\beta^2 e^{\alpha l_b}}{(\beta^2-\alpha^2)}\right]. \tag{A20}$$

[1] J. H. Burroughes *et al.*, Nature **347**, 539 (1990).
[2] J. H. Burroughes, C. A. Jones, and R. H. Friend, Nature **335**, 137 (1988).
[3] I. D. Parker *et al.*, Appl. Phys. Lett. **62**, 1519 (1993).
[4] D. Fichou *et al.*, Adv. Mater. **6**, 64 (1994).
[5] S. Glenis *et al.*, Thin Solid Films **111**, 93 (1984).
[6] J. J. M. Halls *et al.*, Nature **376**, 498 (1995).
[7] J. J. M. Halls *et al.*, Appl. Phys. Lett. **68**, 3120 (1996).
[8] P. Bäuerle *et al.*, Angew. Chem. Int. Ed. Engl. **32**, 76 (1993).
[9] P. Bäuerle *et al.*, J. Am. Chem. Soc. **115**, 10 217 (1993).
[10] F. Devreux, Europhys. Lett. **1**, 233 (1986).
[11] F. Devreux, Synth. Met. **17**, 129 (1987).
[12] M. G. Harrison *et al.*, Synth. Met. **67**, 215 (1994).
[13] O. Dorokhov and N. Kirova, Synth. Met. **57**, 4579 (1993).
[14] N. Kirova and S. Brazovskii, Synth. Met. **76**, 229 (1996).
[15] K. C. Yee and R. R. Chance, J. Polym. Sci. Polym. Phys. Ed. **16**, 431 (1978).
[16] G. Weiser, Phys. Rev. B **45**, 14 076 (1992).
[17] H.-H. Hörhold and J. Opfermann, Makromol. Chem. **131**, 105 (1970).
[18] S. Tokito *et al.*, Jpn. J. Appl. Phys. **25**, 2680 (1986).
[19] T. Takiguchi *et al.*, Synth. Met. **17**, 657 (1987).
[20] K. Pichler *et al.*, J. Phys. Condens. Matter **5**, 7155 (1993).
[21] C. H. Lee, G. Yu, and A. J. Heeger, Phys. Rev. B **47**, 15 543 (1993).
[22] R. N. Marks *et al.*, J. Phys. Condens. Matter **6**, 1379 (1994).
[23] W. Rieβ *et al.*, J. Lumin. **60-61**, 906 (1994).
[24] K. Pakbaz *et al.*, Synth. Met. **64**, 295 (1994).

[25] K. C. Kao and W. Hwang, *Electrical Transport in Solids* (Pergamon, Oxford, 1979), pp. 386–465.
[26] P. M. Borsenberger and D. S. Weiss, *Organic Receptors for Imaging Systems* (Dekker, New York, 1993).
[27] M. G. Harrison and J. Grüner, in ICSM '96 [Synth. Met. (to be published)].
[28] M. G. Harrison, J. Grüner, and G. C. W. Spencer, Synth. Met. **76**, 71 (1996).
[29] M. Gailberger and H. Bässler, Phys. Rev. B **44**, 8643 (1991).
[30] A. K. Ghosh *et al.*, J. Appl. Phys. **45**, 230 (1974).
[31] C. W. Tang and A. C. Albrecht, J. Chem. Phys. **62**, 2139 (1975).
[32] H. B. DeVore, Phys. Rev. **102**, 86 (1956).
[33] A. K. Ghosh and T. Feng, J. Appl. Phys. **49**, 5982 (1978).
[34] A. Désormeaux, J. J. Max, and R. M. Leblanc, J. Phys. Chem. **97**, 6670 (1993).
[35] P. Dannetun *et al.*, Synth. Met. **55**, 212 (1993).
[36] P. Dannetun *et al.*, J. Chem. Phys. **100**, 6765 (1994).
[37] C. Frederiksson *et al.*, Synth. Met. **57**, 4632 (1993).
[38] R. F. Chaiken and D. R. Kearns, J. Chem. Phys. **45**, 3966 (1966).
[39] G. R. Johnston and L. E. Lyons, Aust. J. Chem. **23**, 1571 (1970).
[40] C. Catry *et al.*, Makromol. Chem. Macromol. Chem. Phys. **194**, 2985 (1993).
[41] E. Frankevich *et al.*, Phys. Rev. B **53**, 4498 (1996).
[42] A. Köhler (private communication).
[43] H. Antoniadis *et al.*, Phys. Rev. B **50**, 14 911 (1994).
[44] R. Kersting *et al.*, Phys. Rev. Lett. **73**, 1440 (1994).
[45] V. I. Arkhipov *et al.*, Phys. Rev. B **52**, 4932 (1995).
[46] M. Deussen, M. Scheidler, and H. Bässler, Synth. Met. **73**, 123 (1995).
[47] P. J. Hamer, Ph.D. thesis, University of Cambridge, 1996.
[48] P. G. Dacosta and E. M. Conwell, Phys. Rev. B **48**, 1993 (1993).
[49] E. M. Conwell and H. A. Mizes, Synth. Met. **69**, 613 (1995).
[50] J. M. Leng *et al.*, Phys. Rev. Lett. **72**, 156 (1994).
[51] C. H. Lee *et al.*, Phys. Rev. B **49**, 2396 (1994).
[52] I. H. Campbell *et al.*, Phys. Rev. Lett. **76**, 1900 (1996).
[53] G. J. Lee *et al.*, Synth. Met. **69**, 431 (1995).
[54] B. Tian *et al.*, J. Chem. Phys. **95**, 3191 (1991).
[55] O. Lhost and J. L. Brédas, J. Chem. Phys. **96**, 5279 (1992).
[56] H. S. Woo *et al.*, Synth. Met. **59**, 13 (1993).
[57] P. Papanek *et al.*, Phys. Rev. B **50**, 15 668 (1994).
[58] M. Fahlman *et al.*, Macromolecules **28**, 1959 (1995).
[59] J. H. F. Martens *et al.*, Synth. Met. **41**, 301 (1991).
[60] J. Ma *et al.*, Phys. Rev. B **44**, 11 609 (1991).
[61] G. Mao *et al.*, J. Chem. Phys. **98**, 712 (1992).
[62] W. Liang and F. E. Karasz, Polymer **34**, 2702 (1993).
[63] B. Mollay *et al.*, Phys. Rev. B **50**, 10 769 (1994).
[64] G. R. Hayes, I. D. W. Samuel, and R. T. Phillips, Phys. Rev. B **52**, R11 569 (1995).
[65] U. Rauscher, H. Bässler, and D. D. C. Bradley, Phys. Rev. B **42**, 9830 (1990).
[66] S. Heun *et al.*, J. Phys. Condens, Matter **5**, 247 (1993).
[67] N. T. Harrison *et al.*, Phys. Rev. B **53**, 15 815 (1996).
[68] N. Karl, A. Bauer *et al.*, Mol. Cryst. Liq. Cryst. **252**, 243 (1994).
[69] K. Herrmann and O. Gerngross, Kautschuk **8**, 181 (1932).
[70] W. M. D. Bryant, J. Polym. Sci. **2**, 547 (1947).
[71] D. R. Gagnon *et al.*, Synth. Met. **20**, 85 (1987).
[72] M. A. Masse *et al.*, J. Mater. Sci. **25**, 311 (1990).
[73] X. B. Zhang *et al.*, Macromolecules **29**, 1554 (1996).
[74] N. C. Greenham, Proc. SPIE Int. Soc. Opt. Eng. **1910**, 111 (1993).
[75] M. Yan *et al.*, Phys. Rev. Lett. **73**, 744 (1994).
[76] P. J. Hamer *et al.*, Philos. Mag. B **73**, 367 (1996).
[77] C. Taliani and L. M. Blinov, Adv. Mater. **8**, 353 (1996).
[78] E. L. Frankevich *et al.*, Phys. Rev. B **46**, 9320 (1992).
[79] A. Köhler *et al.*, in ICSM '96 [Synth. Met. (to be published)].
[80] M. Yan *et al.*, Phys. Rev. Lett. **72**, 1104 (1994).
[81] H. A. Mizes and E. M. Conwell, Phys. Rev. B **50**, 11 243 (1994).
[82] H. A. Mizes and E. M. Conwell, Synth. Met. **68**, 145 (1995).
[83] I. B. Berlman, J. Phys. Chem. **74**, 3085 (1970).
[84] N. C. Greenham *et al.*, Chem. Phys. Lett. **241**, 89 (1995).
[85] L. J. Rothberg *et al.*, Synth. Met. **78**, 231 (1996).
[86] J. Grüner *et al.*, Synth. Met. **67**, 181 (1994).
[87] G. Grem *et al.*, Synth. Met. **71**, 2193 (1995).
[88] A. Köhler *et al.*, Chem. Phys. Lett. **243**, 456 (1995).
[89] G. H. Gelinck, J. M. Warman, and E. G. J. Staring, J. Phys. Chem. **100**, 5485 (1996).
[90] A. R. Brown, D. M. Deleeuw, E. E. Havinga *et al.*, Synth. Met. **68**, 65 (1994).
[91] A. Dodabalapur, L. Torsi, and H. E. Katz, Science **268**, 270 (1995).
[92] L. Torsi, A. Dodabalpur, and H. E. Katz, J. Appl. Phys. **78**, 1088 (1995).
[93] F. Garnier *et al.*, J. Am. Chem. Soc. **115**, 8716 (1993).
[94] A. K. Ghosh and T. Feng, J. Appl. Phys. **44**, 2781 (1973).
[95] B. A. Gregg, M. A. Fox, and A. J. Bard, J. Phys. Chem. **94**, 1586 (1990).